



Turning complexity into clarity.
Powerful, configurable Guava® flow cytometers.

EMD Millipore Corp. is a subsidiary of Merck KGaA, Darmstadt, Germany.



Guava easyCyte™ Flow Cytometers

Request Demo



A Heterozygous *RAB27A* Mutation Associated with Delayed Cytolytic Granule Polarization and Hemophagocytic Lymphohistiocytosis

This information is current as of March 7, 2016.

Mingce Zhang, Claudia Bracaglia, Giusi Prencipe, Christina J. Bemrich-Stolz, Timothy Beukelman, Reed A. Dimmitt, W. Winn Chatham, Kejian Zhang, Hao Li, Mark R. Walter, Fabrizio De Benedetti, Alexei A. Grom and Randy Q. Cron

J Immunol 2016; 196:2492-2503; Prepublished online 15 February 2016;
doi: 10.4049/jimmunol.1501284
<http://www.jimmunol.org/content/196/6/2492>

-
- Supplementary Material** <http://www.jimmunol.org/content/suppl/2016/02/12/jimmunol.1501284.DCSupplemental.html>
- References** This article **cites 48 articles**, 16 of which you can access for free at:
<http://www.jimmunol.org/content/196/6/2492.full#ref-list-1>
- Subscriptions** Information about subscribing to *The Journal of Immunology* is online at:
<http://jimmunol.org/subscriptions>
- Permissions** Submit copyright permission requests at:
<http://www.aai.org/ji/copyright.html>
- Email Alerts** Receive free email-alerts when new articles cite this article. Sign up at:
<http://jimmunol.org/cgi/alerts/etoc>

The Journal of Immunology is published twice each month by
The American Association of Immunologists, Inc.,
9650 Rockville Pike, Bethesda, MD 20814-3994.
Copyright © 2016 by The American Association of
Immunologists, Inc. All rights reserved.
Print ISSN: 0022-1767 Online ISSN: 1550-6606.



A Heterozygous *RAB27A* Mutation Associated with Delayed Cytolytic Granule Polarization and Hemophagocytic Lymphohistiocytosis

Mingce Zhang,* Claudia Bracaglia,[†] Giusi Prencipe,[†] Christina J. Bemrich-Stolz,[‡] Timothy Beukelman,*[§] Reed A. Dimmitt,[¶] W. Winn Chatham,[§] Kejian Zhang,^{||} Hao Li,[§] Mark R. Walter,[#] Fabrizio De Benedetti,[†] Alexei A. Grom,** and Randy Q. Cron*^{•§}

Frequently fatal, primary hemophagocytic lymphohistiocytosis (HLH) occurs in infancy resulting from homozygous mutations in NK and CD8 T cell cytolytic pathway genes. Secondary HLH presents after infancy and may be associated with heterozygous mutations in HLH genes. We report two unrelated teenagers with HLH and an identical heterozygous *RAB27A* mutation (c.259G→C). We explore the contribution of this Rab27A missense (p.A87P) mutation on NK cell cytolytic function by cloning it into a lentiviral expression vector prior to introduction into the human NK-92 cell line. NK cell degranulation (CD107a expression), target cell conjugation, and K562 target cell lysis was compared between mutant- and wild-type-transduced NK-92 cells. Polarization of granzyme B to the immunologic synapse and interaction of mutant Rab27A (p.A87P) with Munc13-4 were explored by confocal microscopy and proximity ligation assay, respectively. Overexpression of the *RAB27A* mutation had no effect on cell conjugate formation between the NK and target cells but decreased NK cell cytolytic activity and degranulation. Moreover, the mutant Rab27A protein decreased binding to Munc13-4 and delayed granzyme B polarization toward the immunologic synapse. This heterozygous *RAB27A* mutation blurs the genetic distinction between primary and secondary HLH by contributing to HLH via a partial dominant-negative effect. *The Journal of Immunology*, 2016, 196: 2492–2503.

Familial, or primary, hemophagocytic lymphohistiocytosis (fHLH) is an often fatal rare disorder of infancy resulting from dysregulation of the immune response (1). fHLH occurs in approximately 1 in 50,000 live births, as it is frequently a result of homozygous mutations in autosomal recessive genes

encoding proteins involved in lymphocyte cytolytic activity (e.g., Munc13-4, Rab27A, perforin, Syntaxin 11, Munc18-2) (2), resulting in excessive immune activation or ineffective dampening of an immune response to infectious organisms (3, 4). Criteria to establish the diagnosis of fHLH are either known homozygous genetic mutations in fHLH genes or the presence of five of eight of the following: fever; splenomegaly; cytopenias affecting at least two of three cell lines; hypertriglyceridemia and/or hypofibrinogenemia; hemophagocytosis in lymph nodes, bone marrow, or spleen; low or absent NK cell cytolytic activity; hyperferritinemia; and high levels of soluble (s)CD25 (IL-2R α -chain) (5). Following the diagnosis, most patients are treated with the etoposide-based HLH-2004 protocol. The predecessor of HLH-2004, the HLH-94 protocol and subsequent bone marrow transplantation, has been associated with a 45% mortality rate for primary and secondary forms of HLH (6).

Secondary forms of HLH (sHLH) frequently result from a reactive process to a number of infectious and oncologic conditions (5). When the same process occurs in the setting of rheumatic disease, it is termed macrophage activation syndrome (MAS) (7). fHLH criteria are often too restrictive for a timely diagnosis of sHLH or MAS. Attempts to develop disease-specific sHLH/MAS criteria have been proposed but these are limited to a few diseases (8). Most recently, propensity scores for all forms of sHLH and MAS have been proposed that are not disease-specific, but have yet to be validated (9).

Treatment for sHLH and MAS often vary widely from etoposide-based protocols to more traditional immunosuppressive approaches. Treatment of sHLH and MAS includes high dose corticosteroids (CS), i.v. Ig, and cyclosporine A (CsA) (7, 10). Recently, in uncontrolled reports, the rIL-1R antagonist (rIL-1Ra), anakinra, appears highly effective and well tolerated for rheumatic disease-associated MAS

*Division of Pediatric Rheumatology, University of Alabama at Birmingham, Birmingham, AL 35233; [†]Divisione di Reumatologia Pediatrica, Ospedale Pediatrico Bambino Gesù, 00165 Rome, Italy; [‡]Division of Pediatric Hematology–Oncology, University of Alabama at Birmingham, Birmingham, AL 35233; [§]Division of Clinical Immunology and Rheumatology, University of Alabama at Birmingham, Birmingham, AL 35294; [¶]Division of Pediatric Gastroenterology, University of Alabama at Birmingham, Birmingham, AL 35233; ^{||}Human Genetics, University of Cincinnati, Cincinnati, OH 45229; [#]Department of Microbiology, University of Alabama at Birmingham, Birmingham, AL 35294; and **Division of Pediatric Rheumatology, University of Cincinnati, Cincinnati, OH 45229

ORCID: 0000-0002-4720-5471 (H.L.).

Received for publication June 10, 2015. Accepted for publication January 12, 2016.

This work was supported by grants from the Kaul Pediatric Research Institute (to R.Q.C.) and by National Institutes of Health Grants R01 AR059049 (to A.A.G.) and R01 AI097629 and R01 AI049342 (to M.R.W.). The University of Alabama at Birmingham Immunology Flow Cytometry Core Facility, which was used for this study, was supported by National Institute of Arthritis and Musculoskeletal and Skin Diseases Grant P30 AR048311.

Address correspondence and reprint requests to Dr. Randy Q. Cron, University of Alabama at Birmingham, Children's Park Place, Suite 210, 1601 4th Avenue South, Birmingham, AL 35233. E-mail address: rcron@peds.uab.edu

The online version of this article contains supplemental material.

Abbreviations used in this article: ALT, alanine aminotransferase; AST, aspartate aminotransferase; CRP, C-reactive protein; CS, corticosteroid; CsA, cyclosporine A; FCM, flow cytometry; fHLH, familial hemophagocytic lymphohistiocytosis; HA, hemagglutinin; HLH, hemophagocytic lymphohistiocytosis; LDH, lactate dehydrogenase; MAS, macrophage activation syndrome; PLA, proximity ligation assay; rIL-1Ra, rIL-1R antagonist; s, soluble; sHLH, secondary hemophagocytic lymphohistiocytosis; WT, wild-type.

Copyright © 2016 by The American Association of Immunologists, Inc. 0022-1767/16/\$30.00

refractory to standard treatment (11–16). Mortality for sHLH and MAS treated by these approaches ranges from 0 to 14%; this is remarkably low despite the fact that many of these patients possess heterozygous mutations in fHLH genes that are also present in patients treated with the etoposide-based protocol (14, 17).

Of late, the genetics of sHLH and MAS have been more fully explored. Munc13-4 (*UNC13D*) gene polymorphisms (18) and a mutation (19), as well as perforin mutations (20), have all been associated with MAS in systemic juvenile idiopathic arthritis patients. Furthermore, a variety of heterozygous mutations in fHLH genes have been identified in a significant number of children (17, 21) and adults (22, 23) with sHLH and MAS. Moreover, overexpression in a NK cell line of a novel *STXBP2* missense mutation from a patient with sHLH was recently demonstrated to decrease cytolytic capacity (17). Similarly, other heterozygous *STXBP2* mutations in patients with sHLH were elegantly shown to act in a dominant-negative fashion to impair lytic granule fusion to the cell membrane with defective perforin-mediated cytotoxicity (24). Most recently, it has been reported that defective perforin-mediated cell lysis by NK cells and CD8 T cells results in prolonged interaction between the cytotoxic cell and the Ag-presenting targeting cell, and this contributes to a proinflammatory cytokine storm responsible for the clinical features associated with HLH (25). Thus, fHLH gene mutations in cytotoxic pathway genes that disrupt or delay cytotoxicity likely directly contribute to HLH pathology even in individuals with complete or partial dominant-negative heterozygous mutations.

In this study, we explore the effect of a heterozygous *RAB27A* missense mutation (*c.259G→C*) on NK cell cytotoxic function. This variant is listed in the Single Nucleotide Polymorphism database as rs104894497 (<http://www.ncbi.nlm.nih.gov/projects/SNP/>), and the minor allele frequency in the Exome Aggregation Consortium database (<http://exac.broadinstitute.org/>) is 0.02% in a European population. This *Rab27A* p.A87P mutation was identified in two unrelated patients who developed sHLH later in life during their teenage years. Both patients responded well to immunosuppression with CS and CsA, with or without rIL-1Ra, avoiding the toxicity and morbidity associated with etoposide-based protocols. These disease-contributing single copy fHLH-associated gene mutations from sHLH patients blur the genetic distinction between fHLH and sHLH. Moreover, this suggests that a much larger proportion of the general population may be at risk for sHLH development if only one mutant copy can contribute to delayed cytotoxic activity. Finally, despite the genetic contribution to sHLH and MAS shared with fHLH, these patients pose the question as to whether less toxic immunosuppression-based treatments may be preferred to etoposide-containing regimens as first line therapy for sHLH and MAS patients.

Materials and Methods

Patient data

Data pertaining to clinical course, laboratory values, and treatment were abstracted from patients' electronic medical records. The patients' PBMCs were sequenced for the following HLH genes: *UNC13D*, *PRF1*, *STX11*, *STXBP2*, and *RAB27A*. The *RAB27A* mutation was confirmed by DNA sequencing as described (23) using DNA obtained from a buccal swab from the American patient and from both of her parents, as well as from peripheral blood of the Italian patient, his sibling, and both of his parents. There was no family history of autoimmunity, autoinflammatory disease, or unexplained febrile deaths in the families, and no extended *RAB27A* genotyping was carried out beyond the patients, parents, and sibling.

DNA constructs

cDNAs encoding wild-type (WT) human *Rab27A* and Munc13-4 were generated by reverse transcription from RNA of the human NK-92 NK cell

line (26). The cDNAs were cloned into expression vectors and the WT sequences were confirmed by DNA sequencing. The patient-derived *RAB27A* mutant cDNA (*c.259G→C*) was generated from the WT *RAB27A* cDNA by site-directed mutagenesis as described (27) and confirmed by DNA sequencing. The lentiviral expression vector, z-368- Δ NP, and the packaging plasmid, Δ 8.91, were provided by Dr. Philip Zoltick (The Children's Hospital of Philadelphia) (28). Both WT and mutant *RAB27A* cDNAs were independently subcloned into z-368- Δ NP to help generate recombinant lentiviruses. These viruses were separately transduced into NK-92 cells as detailed below. Transduction efficiencies were monitored by coexpression of GFP as detected by flow cytometry (FCM). For protein–protein interaction assays, a FLAG tag–fused *UNC13D* cDNA and hemagglutinin (HA) tag–fused WT and mutant *RAB27A* cDNAs were subcloned into z-368- Δ NP by a 2A viral linker. Both the FLAG tag and HA markers were coupled to the 3' ends (carboxyl-terminals) of the respective proteins and represented exogenous versions of Munc13-4 or *Rab27A* in the transduced NK-92 cells studied.

Abs and probes

The anti-human CD56-PE-Cy7 and CD107a-PE mAbs were purchased from eBioscience (San Diego, CA). The anti-human granzyme B–allophycocyanin Ab was from BD Biosciences (San Jose, CA), and the rabbit Ab against GFP was from Invitrogen (Grand Island, NY). F-actin and granzyme B were also detected with phalloidin conjugated with Alexa Fluor 555 (Invitrogen) and anti-granzyme B conjugated to Alexa Fluor 647 (Invitrogen), respectively. The anti-FLAG rabbit Abs were purchased from Cell Signaling Technology (Beverly, MA), and the anti-HA mouse mAb was obtained from Abcam (Cambridge, MA). Fluorochrome-tagged anti-perforin and anti-IFN- γ were from BD Biosciences and eBioscience, respectively. For the in situ proximity ligation assay (PLA), the probes, anti-rabbit PLUS and anti-mouse MINUS, and the Texas Red–conjugated detection reagents were purchased from Sigma-Aldrich (St. Louis, MO). For the Western blot assays, rabbit anti-HA and chicken anti-FLAG Abs were obtained from Abcam. The rabbit anti- β -actin and anti-rabbit IgG Alexa Fluor 680–conjugated polyclonal Abs were purchased from Invitrogen, and the IRDye 800CW donkey anti-chicken IgG was bought from LI-COR Biosciences (Lincoln, NE).

Lentiviral preparation and transduction

HEK293T cells were transfected with the respective z-368- Δ NP–expression constructs along with Δ 8.91 and pVSV-G using the FuGENE HD transfection reagent (Roche, Branford, CT). Lentiviral production was concentrated using the Lenti-X concentrator reagent (Clontech, Mountain View, CA). NK-92 cells were infected with lentiviruses overnight at a multiplicity of infection of 50:1. Transduction efficiency was between 45 and 55% at day 5 and afterward for up to 4 wk. All assays were performed between 2 and 3 wk following lentiviral infection.

Cytotoxicity and degranulation assays

The NK-sensitive K562 erythroleukemia target cells (29) were labeled by the cell tracer dye eFluor 450 (eBioscience) 12 h prior to the cytotoxicity assay. The GFP-expressing, lentiviral-transduced NK-92 cells and labeled K562 target cells were mixed together at different E:T cell ratios and incubated at 37°C for 4 h in the presence (24 h preincubation) or absence of rIL-6 (10–50 ng/ml). The cells were then stained with Live/Dead near-IR dye (Invitrogen) and analyzed by FCM (LSR II, BD Biosciences). For cytotoxicity assays using patient and control frozen peripheral blood samples, PBMCs were thawed and cultured in RPMI 1640 media with 10% heat-inactivated FBS (HyClone Laboratories, Logan, UT) and rIL-2 (50 U/ml) for 24 h. Then, K562 cells were loaded with bis(acetoxymethyl) 2,2':6',2''-terpyridine-6,6''-dicarboxylate (PerkinElmer, Waltham, MA) and mixed with Ficoll-separated PBMCs at E:T ratios of 6:1 to 100:1 for 3 h prior to measuring lysis by EuTDA fluorescence.

For degranulation assays, the transduced NK-92 cells were mixed with K562 cells at a 2:1 E:T ratio and incubated between 0 and 4 h in the presence of fluorochrome-conjugated anti-CD107a Ab. K562 target cells served as a stimulus for NK-92 cell degranulation. To identify NK-92 effector cells, cells were either labeled with CFSE 12 h prior to degranulation assays or stained with fluorochrome-conjugated anti-CD56 mAb after incubation with K562 stimulator cells. CD107a cell surface expression on NK-92 cells was detected by FCM as described by others (30). For degranulation assays involving patient and control frozen peripheral blood samples, PBMCs were thawed and cultured as above, and Ficoll-separated PBMCs were incubated with K562 cells for 3 h at E:T ratios of 10:1 to 1:3 in the presence of anti-CD107a Ab. NK cells were identified with mAb against CD56 (NK cells) and CD3 (T cells gated out).

Intracellular perforin and IFN- γ levels

PBMCs were isolated from the Italian patient and controls by Ficoll separation and then were frozen. Cells were thawed and cultured at a density of 1×10^6 cells/ml in RPMI 1640 medium supplemented with 10% FBS, with or without human IL-6 (10 ng/ml) and soluble human IL-6 receptor (125 ng/ml). After 24 h of incubation at 37°C in the presence or absence of IL-6/sIL-6R, IL-2 (50 U/ml) was added to the medium and cells were incubated for another 24 h. Intracellular perforin expression levels in the NK cell subset (CD56⁺CD3⁻) were evaluated by FCM as previously described (31). For intracellular detection of IFN- γ , Rab27A (WT or mutant)-transduced GFP⁺ NK-92 cells were incubated 1:1 with K562 cells for 4 h prior to detection of intracellular IFN- γ by FCM as described (31).

Cell-cell conjugation assays

The GFP-expressing lentiviral-transduced NK-92 cells were mixed with cell tracer dye (eFluor 450)-labeled K562 cells and centrifuged for 30 s at a very low speed. Cells were incubated at 37°C for 0, 15, 30, 60, 120, 240, or 480 min and then fixed with a 1% paraformaldehyde solution. Conjugates between NK-92 cells and K562 cells were detected by two-color FCM and analyzed using FlowJo 8.8.6 software (Tree Star, Ashland, OR).

Structural modeling

Modeling and figure generation (see Fig. 4) of Rab27A p.A87P bound to WT Slp2-a and WT melanophilin was performed using the PyMOL molecular graphics system software package (DeLano Scientific, San Carlos, CA) using prior published Rab27A WT structures (32, 33).

Proximity ligation assay

NK-92 cells were infected with a FLAG-tagged WT Munc13-4-expressing lentivirus, and transfected cells were sorted by coexpression of GFP. Cells were expanded in vitro and FLAG tag expression was confirmed by intracellular staining and FCM. NK-92 cells were superinfected with an HA-tagged WT or mutant (p.A87P) Rab27A-expressing lentivirus. Exogenous Rab27A expression was confirmed by intracellular staining against the HA tag. Proximity of the proteins, a surrogate of protein-protein interaction, was detected by the Duolink method as per the manufacturer's instructions (Sigma-Aldrich). Dual lentivirus-expressing NK-92 cells were mixed 1:1 with K562 cells for 30 min at 37°C to activate the cytolytic pathway. Cells were cytospun onto glass slides and fixed with 1% paraformaldehyde. Fixed cells were stained with polyclonal rabbit anti-FLAG (Munc13-4) Abs and a mouse anti-HA (Rab27A) mAb for 1 h prior to two washes. Cells were then incubated for 1 h with anti-rabbit PLA and anti-mouse PLA containing complementary proprietary PCR primers. Cells were washed twice and ligation solution was added for 30 min. Cells were washed again prior to addition of amplification solution for 100 min. Slides were sealed and images were taken with an Olympus BX41 camera. Single protein interactions were visualized using fluorescence and bright-field images, and the numbers of PLA particles per cell were counted and averaged for 100 cells per condition (blinded to the counter, M.Z.).

Coimmunoprecipitation assays

WT Munc13-4-FLAG-expressing NK-92 cells were sorted by GFP coexpression and superinfected with lentiviruses expressing empty vector control, WT Rab27A-HA, or mutant Rab27A p.A87P-HA. The transduced NK-92 cells were stimulated with K562 cells at a ratio of 1:1 for 0, 2, and 6 h prior to cell lysis for immunoprecipitation. FLAG immunoprecipitation kits purchased from Sigma-Aldrich were used as per the manufacturer's guidelines. For Western blots, cell lysates and immunoprecipitated proteins were electrophoresed on Mini-Protean TGX gels from Bio-Rad (Hercules, CA) under denatured or native conditions. In the blotting process, rabbit anti-HA and chick anti-FLAG were used to detect HA- and FLAG-conjugated proteins, respectively, followed by anti-rabbit IgG Ab conjugated with Alexa Fluor 680 and donkey anti-chicken IgG conjugated with IRDye 800CW. Use of an Odyssey infrared imager (LI-COR Biosciences) was provided by Dr. John Mountz (University of Alabama at Birmingham, Birmingham, AL) and used to scan the blotted signals on the polyvinylidene fluoride membranes. ImageJ2 software (National Institutes of Health, Bethesda, MD) was used to measure band intensity.

Confocal imaging assays

For immune synapse imaging assays, the lentiviral-transduced NK-92 cells were mixed with CFSE (Life Technologies, Grand Island, NY)-labeled K562 target cells and incubated for 30 min at 37°C. Cells were then spun down to a glass slide using a cytospin instrument and fixed using a 1% paraformaldehyde solution. Immunofluorescence staining of granzyme B

and F-actin distributions within cells was accomplished with fluorochrome-labeled anti-granzyme B mAb and phallotoxins (34), respectively. To enhance the imaging, Alexa Fluor 488 (Life Technologies)-labeled anti-GFP mAb was included for intracellular staining. For granzyme B polarization assays, NK-92 effector cells and K562 target cells were mixed at a 1:1 ratio and incubated for different time periods (0–8 h) before fluorescent staining of granzyme B and cell nuclei (DAPI). Confocal imaging was performed and recorded using a laser scanning microscope with a digital camera (Zeiss, Thornwood, NY). Confocal imaging data were analyzed using the Bioquant system (Bioquant Image Analysis, Nashville, TN). Percentage polarized cells (>75% granzyme B at the immunologic synapse) was calculated by counting 200 cells per time point, per condition in a blinded (time point and condition masked) fashion to the viewer (M.Z.).

Statistical analyses

Statistical analyses were performed with GraphPad Prism 6 (GraphPad Software, La Jolla, CA) software. Two-way ANOVA analysis was used to calculate *p* values ($\alpha = 0.05$) for the NK-92 cell cytotoxicity assay, the granzyme B polarization analyses, and the interaction between Munc13-4 and Rab27A as detected by the PLA.

Study approval

The studies were conducted in accordance with the Declaration of Helsinki principles. Institutional Review Board approval was obtained from the University of Alabama at Birmingham and the Ospedale Pediatrico Bambino Gesù, respectively. Written informed consent for all study aspects, including publication of potentially identifiable material, was obtained from the patients and their respective parents.

Results

Clinical histories

A previously healthy 18-y-old white American female was admitted to the hospital on the gastroenterology service for 2 wk of fever and abdominal pain. On examination her liver and spleen were notably enlarged, she was hypertensive, and her mental status was decreased. Her laboratory findings were notable for pancytopenia (WBC, 1720 cells/ μ L; hemoglobin, 10.9 mg/dl; platelets,

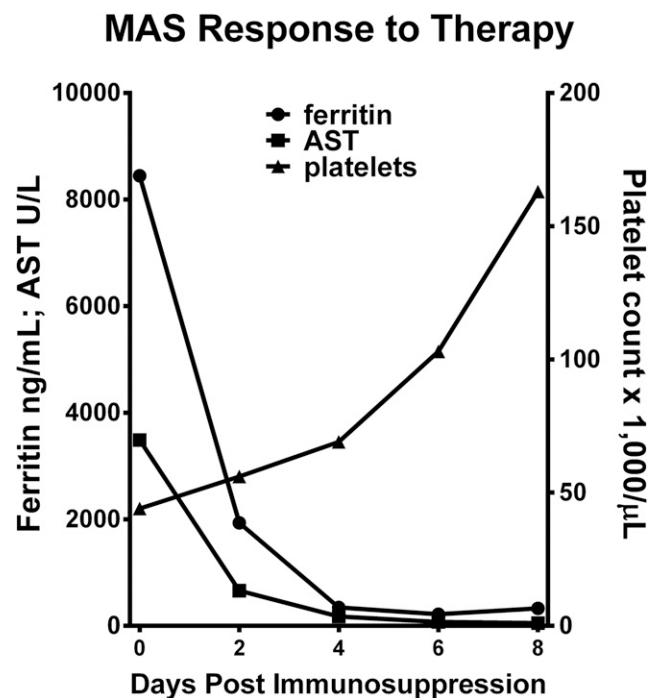


FIGURE 1. Rapid clinical response of sHLH to immunosuppression with high-dose CS, CsA, and anakinra. Serum ferritin (●) and AST (■) levels, as well as circulating platelet counts (▲), are graphed before (day 0) and after immunosuppression (methylprednisolone, CsA, and anakinra/rIL-1Ra) for the American sHLH patient with the heterozygous Rab27A p.A87P missense mutation.

44,000/ μ l), liver failure (albumin, 2.7 mg/dl [\geq 3.7]; aspartate aminotransferase [AST], 3487 IU/l [\leq 30]; alanine aminotransferase [ALT], 2523 IU/L [\leq 35]; aldolase, 61.8 U/l [$<$ 8.1]; triglycerides, 201 mg/dl [\leq 140]), coagulopathy (prothrombin time, 20.7 s [\leq 15.2]; partial thromboplastin time, 59.2 s [\leq 36.0]; D-dimers, 7639 ng/ml [\leq 240]; fibrinogen, 139 mg/dl [164–458]), and inflammation (C-reactive protein [CRP], 5.96 mg/dl [$<$ 1.00]; ferritin, 8446 ng/ml [\leq 115]; sCD25, 4171 U/ml [$<$ 1105]; sCD163, 1718 U/ml [$<$ 1378]). Her NK cell numbers were normal but NK cell function was virtually absent (2% lysis at the 50:1 E:T ratio). An extensive infectious work-up was unrevealing with notably negative or normal evaluations for hepatitis A/B/C, HIV-1, EBV, CMV, *Ehrlichia chaffeensis*, and enterovirus. Her anti-nuclear Ab test was negative, but her serum complement levels were low (C3, 20 mg/dl [51–95]; C4, 3 mg/dl [8–44]), a feature of MAS (35). The bone marrow biopsy specimen was essentially normal except that CD163 staining revealed increased numbers of activated macrophages. A brain magnetic resonance imaging was normal. She satisfied criteria for HLH with seven of eight features (five required) present (fever, splenomegaly, cytopenia, hypofibrinogenemia, decreased NK cell function, hyperferritinemia, elevated sCD25) (5).

One week into the hospital admission, and just prior to transfer to intensive care for clinical decompensation, she was started on high-dose i.v. methylprednisolone (500 mg twice daily for 5 d), CsA (3.5 mg/kg/d divided twice daily, i.v.), and s.c. anakinra (rIL-1Ra) at 100 mg (1.6 mg/kg) daily. Within 24 h of immunosuppressive therapy, her clinical condition dramatically improved, and her laboratory features of sHLH showed marked improvement (Fig. 1). She was discharged to home on prednisone 60 mg twice daily, CsA 200 mg twice daily, and anakinra 100 mg daily within 6 d of starting therapy. Within 2 wk of leaving the hospital she developed a bilateral symptomatic chronic anterior uveitis that required periocular CS injections for control of inflammation. Three months after leaving the hospital she developed unilateral herpes simplex keratitis that responded to acyclovir therapy. Her daily oral CS had been tapered to off, and by 6 mo she was also off of CsA, as both sHLH and uveitis were in remission. Anakinra was tapered to off within a year but she later developed HLA-B27–negative

spondyloarthritis. She has had no further episodes of sHLH/MAS in the 5 y since her diagnosis.

Her HLH gene testing was negative for coding mutations in *UNC13D*, *PRF1*, *STX11*, and *STXB2*, but she was found to have a single copy missense mutation in *RAB27A* (*c.259G→C*) leading to an amino acid change (p.A87P). This particular mutation (Single Nucleotide Polymorphism database no. 104894497) has been previously reported and is a known cause of Griscelli type 2, an established cause of fHLH when present as a compound heterozygous mutation (36). Because the DNA sample was obtained from peripheral blood, a buccal swab was analyzed for this mutation in the patient and both of her parents. The Rab27A p.A87P mutation was found to be germline in the patient and her father who has not had a known episode of sHLH.

Across the Atlantic Ocean, a previously healthy 15-y-old native Italian male (unrelated to the prior patient) was admitted to the hospital with a 4-wk history of persistent fever (up to 39°C) unresponsive to antipyretics or broad-spectrum antibiotics, diarrhea, vomiting, skin rash, and arthritis. On physical examination he was noted to have a rash, hepatosplenomegaly, and swelling and tenderness of his elbows. Blood tests showed an increase in leukocyte count (16,210 cells/ μ l) with a normal platelet count (261,000 platelets/ μ l) and no evidence of anemia (12.7 g/dl), but signs of liver inflammation (AST, 224 IU/l; ALT, 635 IU/l; lactate dehydrogenase [LDH], 676 IU/l) and systemic inflammation (D-dimers, 2.26 μ g/ml; CRP, 33.23 mg/dl; ferritin, 5896 ng/ml) with an elevated fibrinogen concentration (818 mg/dl). Lumbar puncture was negative, and viral and bacterial cultures were negative. Broad spectrum i.v. antibiotic treatment (ceftriaxone 100 mg/kg/d) was started with no effect on fever or clinical symptoms. Bone marrow biopsy showed increased numbers of activated macrophages, mostly expressing CD163, and pronounced hemophagocytosis. A diagnosis of sHLH was suspected (four fHLH criteria met; sCD25 was not evaluated), and oral CsA (5 mg/kg/d) and i.v. pulse-dose methylprednisolone (1 g/d for 3 d) were administered, followed by oral prednisone (2 mg/kg/d). However, his symptoms did not improve significantly. Laboratory tests showed a rapid rise in ferritin levels (25,770 ng/ml) and hepatic enzyme activity (AST, 816 IU/l; ALT, 932 IU/l; γ -glutamyl transferase,

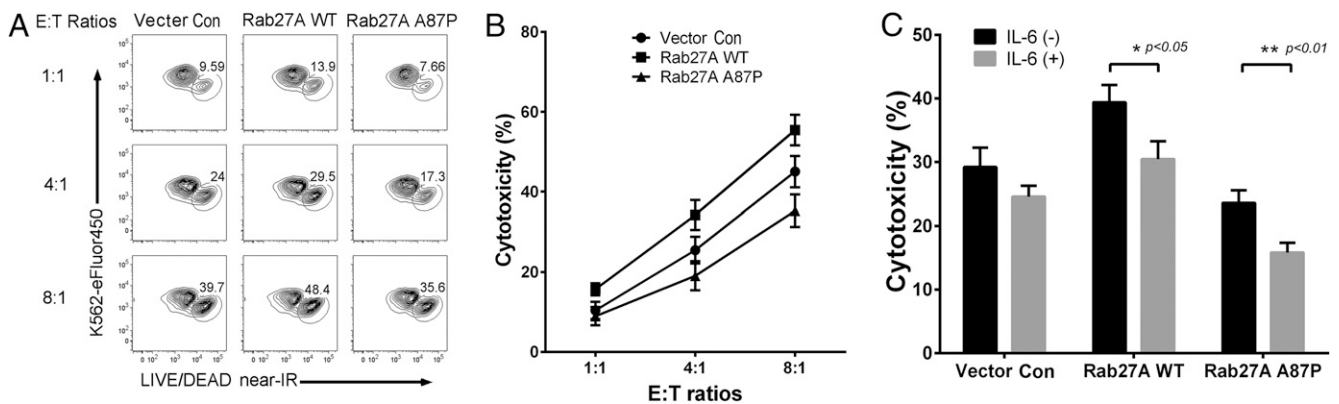


FIGURE 2. Rab27A p.A87P mutation decreases NK cell cytolytic function. (A) eFluor 450–labeled K562 target cells were mixed at increasing E:T ratios with NK-92 cells transduced with lentiviruses expressing empty vector control (*left column*), Rab27A WT (*middle*), or Rab27A p.A87P (*right*) and were incubated for 4 h prior to FCM analysis of K562 cell death. FCM plots were gated on eFluor 450⁺ cells with eFluor 450 depicted on the y-axis, and near-IR staining (dead cells) along the x-axis. One representative experiment is shown with percentages of lysed K562 cells enumerated. (B) Graph showing percentage cytotoxicity at three different E:T ratios for lentivirus-transduced NK-92 cells (empty vector control [●], Rab27A WT [■], and Rab27A p.A87P mutation [▲]). Results are plotted as means \pm SEM for five independent experiments. Two-way ANOVA analysis revealed statistically significant differences ($p < 0.05$) among empty vector–, the Rab27A WT–, and the Rab27A p.A87P mutant–transduced NK-92 cells at all three E:T cell ratios. (C) K562 cytotoxicity (means \pm SEM) from empty vector, WT, or Rab27A p.A87P mutant lentiviral-transduced NK-92 cells in the presence or absence of exogenous IL-6 are shown for a 4:1 E:T ratio. IL-6 significantly decreased cytotoxicity of Rab27A WT (* $p = 0.0175$)– and p.A87P mutant (** $p = 0.0058$)–transduced cells ($n = 3$).

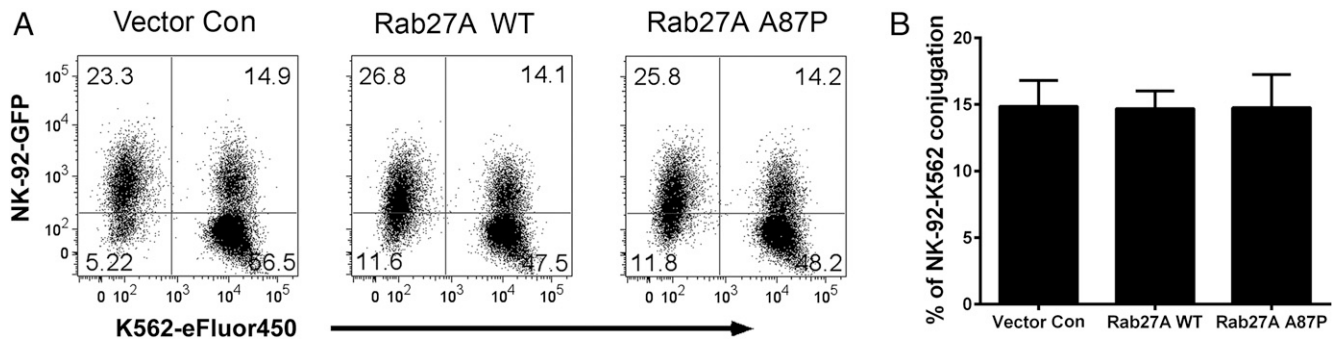


FIGURE 3. Rab27A p.A87P mutation does not alter NK cell conjugate formation with target cells. NK-92 cells transduced with lentiviruses coexpressing GFP and empty vector control (*left*), Rab27A WT (*middle*), or Rab27A p.A87P (*right*) were mixed with eFluor 450–labeled K562 cells and assayed for cell-to-cell conjugation at 30 min as assessed by FCM. **(A)** GFP expression (NK-92 cells) is shown along the y-axis and eFluor 450 fluorescence (K562 cells) is shown along the x-axis. NK-92–K562 cell conjugates are noted in the *upper right quadrants*, and percentages of cells in each quadrant are noted. **(B)** Results shown are representative of three similar experiments, and the means \pm SEM for percentage conjugates are shown in the bar graph to the right.

568 IU/l; LDH, 1629 IU/l), with high fibrinogen (841, mg/dl) and normal triglycerides (141, mg/dl). He did not develop cytopenia, possibly because of the high doses of glucocorticoids. Weekly i.v. cyclophosphamide (500 mg/m² BSA) and dexamethasone (10 mg/m²) were started. His fever disappeared within 48 h after the first infusion and blood tests normalized after the third weekly infusion of cyclophosphamide. Intravenous cyclophosphamide was subsequently administered weekly for the first 5 wk and afterward monthly for 3 mo. Dexamethasone was gradually tapered and discontinued after 4 mo of treatment, and CsA was discontinued after 2 y.

Three years after this first episode, and 1 y after discontinuation of CsA, the patient relapsed with fever, skin rash, arthralgia, and myalgia. Blood examinations revealed normal WBC and platelet counts, no evidence of anemia, mild liver impairment (AST, 33 IU/l; ALT, 78 IU/l; LDH, 451 IU/l), and inflammation (CRP, 13.26 mg/dl; ferritin, 5481 ng/ml; fibrinogen, 707 mg/dl; D-dimers, 0.3 μ g/ml). Bone marrow aspirate showed numerous activated macrophages and hemophagocytosis. Based on his clinical history, a relapse of sHLH was hypothesized, and high doses of oral dexamethasone (10 mg/m²) and oral CsA (4 mg/kg) were started with gradual clinical and laboratory improvement. Dexamethasone was gradually tapered and stopped after 8 mo of treatment while continuing CsA. He has been free of disease for 3 y now. Genetic analysis was negative for mutations in *PRF1*, *UNC13D*, *STX11*, and *STXBP2*, but a single copy missense mutation in *RAB27A* (*c.259G→C*) was identified leading to the same amino acid change (p.A87P) found in the American patient. The Italian patient's father carries the same mutation in Rab27A (p.A87P). Although the father is asymptomatic, he has a baseline moderately high serum ferritin level (800 ng/ml). These two unrelated teenage patients with sHLH prompted our investigation of the functional consequences of a single copy Rab27A missense mutation (p.A87P) on NK cell cytolytic function.

Rab27A p.A87P decreases NK cell cytolytic capacity

Because the American patient's own NK cells had a defect in cytotoxicity, the contribution of her Rab27A p.A87P mutation to decreased cytotoxic activity was explored. Using a lentiviral approach (see *Materials and Methods*), Rab27A WT or mutant Rab27A p.A87P was overexpressed in the human NK cell line NK-92. Lentivirus-transduced NK-92 cells were sorted based on coexpression of GFP and mixed with fluorochrome-labeled K562 target cells at three different E:T cell ratios. Cell death was assessed by FCM using a proprietary dye that enters dead or dying cells. As seen in Fig. 2A, cell death increased with increasing E:T

ratios in all three conditions (empty vector control, Rab27A WT, and Rab27A p.A87P), but NK-92 cytotoxicity of K562 cells increased with overexpression of Rab27A WT, and decreased with overexpression of the patient mutation, Rab27A p.A87P. This effect was seen in repeated experiments (Fig. 2B) and suggested that overexpression of Rab27A p.A87P was able to diminish NK cell cytotoxic capacity. Because it has recently been shown that the inflammatory environment may also contribute to decreased NK cell function (31), the experiment was repeated in the presence or absence of exogenous rIL-6 (37). As seen in Fig. 2C, addition of IL-6 further decreased NK cell cytotoxicity when either WT or mutant Rab27A p.A87P was overexpressed. These studies indicate that a single copy Rab27A p.A87P mutation may diminish NK cell function, and that in a proinflammatory environment this effect will be enhanced.

FCM was next used to explore whether decreased NK cell function was a result of a diminished ability of Rab27A p.A87P-expressing NK cells to form conjugates with the K562 target cells.

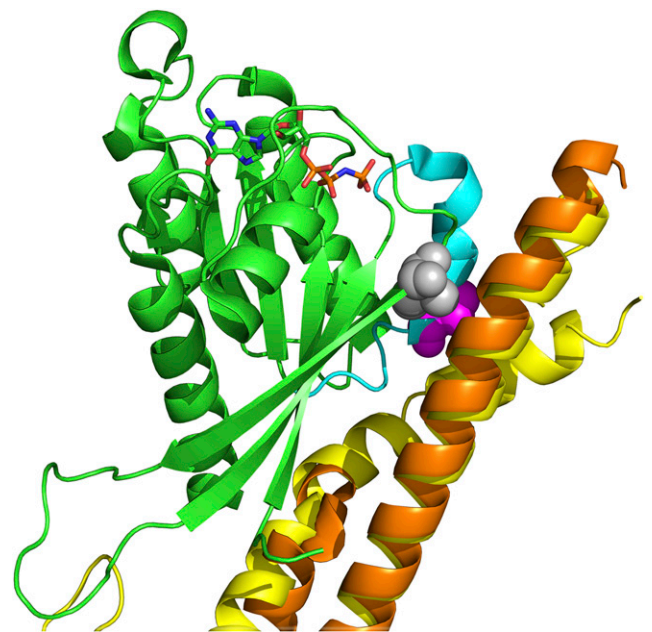


FIGURE 4. The Rab27A p.A87P mutation is located in a putative Rab27A/Munc13-4 binding site. The crystal structure of Rab27A (green) is shown with Munc13-4 homologs, melanophilin (yellow), and Slp2-a (orange). The positions of Rab27A mutations p.A87P (purple) and p.I44T (gray), both of which disrupt binding to WT Munc13-4 *in vitro*, are shown.

Lentivirus-transduced NK-92 cells were detected by GFP expression, and K562 target cells were labeled with the eFluor 450 fluorochrome. As seen in Fig. 3A, the percentage of conjugates (those cell pairs expressing both GFP and eFluor 450, located in the upper right-hand FCM quadrant) were virtually identical when the NK-92 cells were overexpressing Rab27A WT, Rab27A p.A87P, or the empty vector control at 30 min after incubation. This was seen repeatedly ($p > 0.5$) (Fig. 3B). Thus, the Rab27A p.A87P patient mutation had no obvious effect on NK cell-to-target cell conjugate formation at 30 min as assessed by FCM.

Rab27A p.A87P partially disrupts interaction with WT Munc13-4

It had previously been reported that the Rab27A p.A87P mutation completely disrupted the ability of Rab27A to bind Munc13-4 in vitro as evaluated in a mammalian two-hybrid assay (36). We next analyzed in silico the predicted crystal structure of Rab27A p.A87P interactions with Munc13-4 homologs, melanophilin, and Slp2-a. The Rab27A p.A87P mutation is located within the switch 2 region of Rab27A (WT sequence is identical to Rab27B in this region) (Fig. 4). Structural studies on related Rab27B/melanophilin (33) and Rab27A/Slp2-a (32) complexes confirm this switch 2 region of Rab27A as a binding site with Munc13-4. This is confirmed by biochemical analyses that demonstrate disruption of binding to WT Munc13-4 by mutants Rab27A p.A87P (switch 2 mutation) (36) and Rab27A p.I44T (located adjacent to switch 2 on switch 1) (38). Modeling of both the Rab27A p.I44T mutant (gray) and the patients' p.A87P mutation (purple) predict disruption of binding to the Munc13-4 homologs, melanophilin (yellow), and Slp2-a (orange) (Fig. 4).

To test the ability of Rab27A p.A87P to quantitatively bind WT Munc13-4 in situ, we explored this interaction on a per cell basis using the PLA as detailed in *Materials and Methods*. In brief, NK-92 cells were transduced with a lentivirus expressing a FLAG-tagged version of Munc13-4 WT and coexpressing GFP. GFP-sorted NK-92 cells were superinfected with a lentivirus-expressing HA-tagged Rab27A WT, Rab27A p.A87P, or empty vector control. Expression levels were stable over several weeks in culture and roughly equivalent in all conditions (Supplemental Fig. 1). The dually transduced NK-92 cells were incubated with K562 target cells to activate the cytolytic pathway, and the cells

were spun down onto glass slides and paraformaldehyde fixed. The fixed cells were incubated with a rabbit anti-FLAG antisera and a mouse anti-HA mAb. After washes, the cells were incubated with anti-rabbit and anti-mouse Abs, each conjugated with complementary proprietary PCR primers. In situ, NK-92 cells were treated with ligation solution followed by PCR amplification solution containing fluorochrome-tagged DNA complementary to the ligated primers as per the manufacturer's instructions. Intracellular single protein-protein (Rab27A to Munc13-4) interactions were visualized as fluorescent particles and counted using fluorescence microscopy (Fig. 5A). No HA tag was present in the empty vector control, and there were no particles detected, as expected. Interestingly, during the 4-h time course the NK-92 cells transduced with HA-tagged Rab27A p.A87P demonstrated approximately half as many protein-protein interactions with FLAG-tagged Munc13-4 WT as did the NK-92 cells transduced with HA-tagged Rab27A WT (Fig. 5B). This suggests that the Rab27A p.A87P mutation partially disrupts the ability to interact in close proximity with Munc13-4 WT. This was supported by Western blot studies, which revealed decreased coimmunoprecipitation of Rab27A p.A87P (compared with WT Rab27A) with WT Munc13-4 using lysates from transduced NK-92 cells (Supplemental Fig. 2).

Rab27A p.A87P delays granzyme B polarization to the immunologic synapse

As Rab27A and Munc13-4 normally function to help transport granzyme B-containing granules to the NK cell immunologic synapse, the degranulation ability of NK-92 cells transduced with Rab27A p.A87P was explored by examining CD107a cell surface expression. FCM measurement of cell surface CD107a on NK cells is a simple, quick, and reliable method to measure NK cell degranulation (30). NK-92 cells were transduced with a lentivirus expressing Rab27A WT, Rab27A p.A87P, or empty vector control. The cells were next incubated with K562 cells to stimulate cytotoxic granule degranulation as assessed over time by FCM using fluorochrome-conjugated anti-CD107a mAb. As predicted, at the 0 h time point, there is virtually no detectable CD107a expression (1%) on the cell surface of NK-92 cells separately transduced with the three different lentiviruses (Fig. 6A). However, by 2 h post-incubation with K562 cells, CD107a cell surface expression peaked (32%). Overexpression of Rab27A WT augmented degranulation

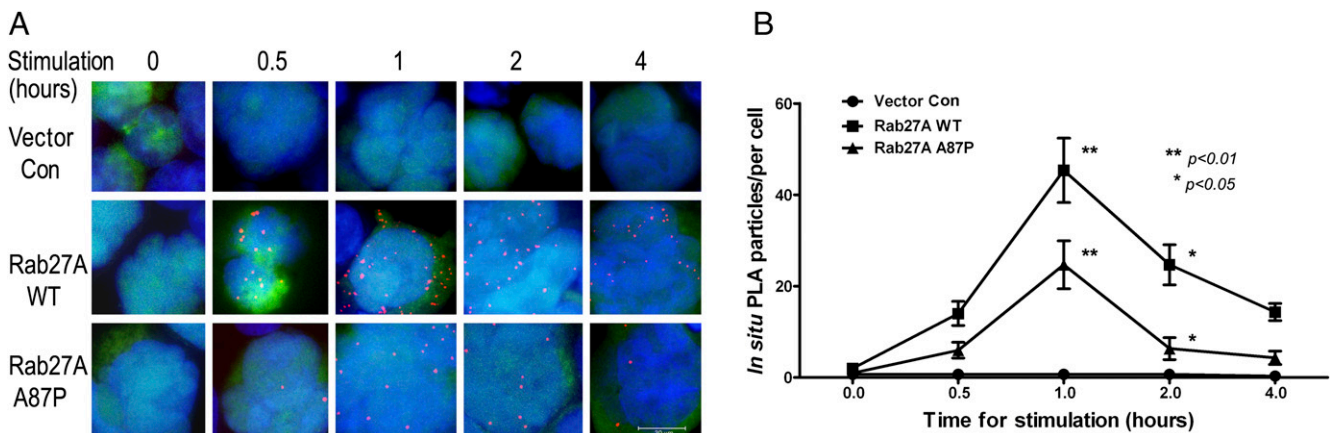


FIGURE 5. Rab27A p.A87P mutation results in decreased interaction with Munc13-4 WT protein. **(A)** NK-92 cells were transduced with a lentivirus expressing FLAG-tagged Munc13-4 WT followed by superinfection with lentiviruses expressing nothing (*top row*) or HA-tagged Rab27A WT (*middle*) or Rab27A p.A87P mutant (*bottom*). The transduced NK-92 cells were stimulated with K562 cells for the indicated time periods prior to in situ PLA as described in *Materials and Methods*. Particles representing protein-protein interactions specifically between transduced Munc13-4 and Rab27A are noted in orange. Scale bar, 30 μ m. **(B)** Results from three independent experiments are summarized and plotted as in situ PLA particles per cell (means \pm SEM) along the y-axis and time of stimulation along the x-axis. Two-way ANOVA analysis showed statistically significant differences ($p < 0.05$) between the means at the 1 and 2 h time points for the Rab27A WT- and Rab27A p.A87P-transduced cells.

compared with administered empty vector control at all the time points analyzed (44% at 2 h), whereas Rab27A p.A87P inhibited CD107a expression in comparison with empty vector for the entire 8-h time course (22% at 2 h) (Fig. 6A, 6B). This implies that Rab27A p.A87P inhibits NK cell cytolytic function by disrupting cytolytic granule polarization to the immunologic synapse with the target cell.

Granzyme B is an effector molecule in CD8 T cell and NK cell cytolytic granules that contributes to target cell apoptosis when delivered via a perforin (also contained in cytolytic granules) pore formed at the immunologic synapse between the lytic cell and the target cell (15, 39). The effect of Rab27A p.A87P on granzyme B polarization to the NK cell immunologic synapse was therefore explored using confocal fluorescence microscopy. GFP and Rab27A dual-expressing lentivirus-transduced NK-92 cells were incubated 1:1 with CFSE-labeled K562 target cells at 37°C for 30 min prior to being spun down onto glass slides and fixed and permeabilized with paraformaldehyde. Cells were then visualized with confocal

microscopy (Fig. 6C). In addition to the GFP (NK-92 cells) and the green nuclear CFSE (K562 cells) stains, both cell types were identified by the addition of phallotoxins (blue) to highlight cytoplasmic actin. Granzyme B (orange to pink) was detected by the addition of fluorochrome-conjugated anti-granzyme B mAb. NK-92 cells transduced with the Rab27A WT lentivirus demonstrated granzyme B polarization to the immunologic synapse with the K562 target cell (Fig. 6C, *top panel*, arrow), whereas Rab27A p.A87P mutant-expressing NK-92 cells did not appear to polarize granzyme B to the synapse formed with the K562 cell (Fig. 6C, *bottom panel*, arrow). We further refined the immunologic synapse by defining the plasma membranes of the transduced NK-92 effector cells and the K562 target cells using directly conjugated and fluorochrome-tagged phalloidin to detect F-actin (Fig. 7). The control-transduced NK-92 cells (effectors) clearly demonstrated granzyme B polarization to the immunologic synapses with adjoining K562 targets, and this appeared augmented when WT Rab27A was overexpressed, and notably diminished when mutant Rab27A p.A87P was transduced

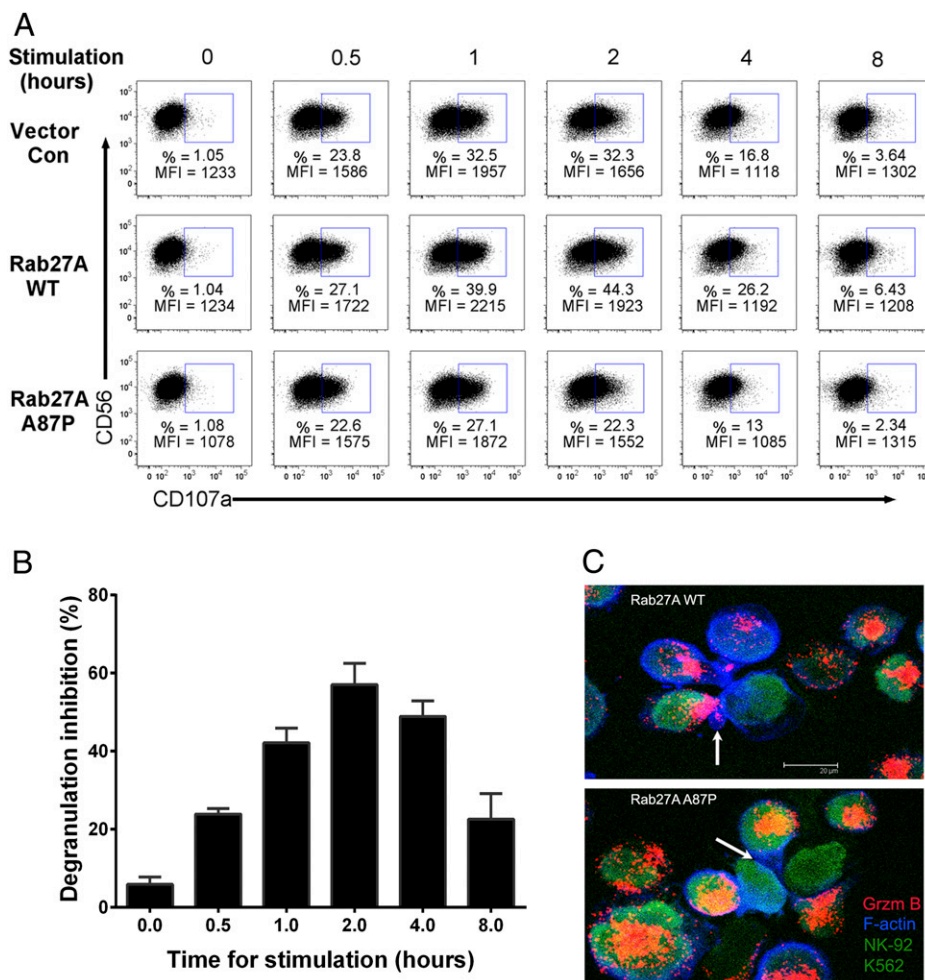


FIGURE 6. Rab27A p.A87P mutation decreases NK cell degranulation and alters cytolytic granule polarization to the immunologic synapse. **(A)** NK-92 cells transduced with lentiviruses expressing empty vector control (*top row*), Rab27A WT (*middle*), or Rab27A p.A87P (*bottom*) were mixed with K562 cells for the indicated times, and cell surface CD107a expression was detected by FCM. One representative set of results from three independent experiments is shown and gated on CD56⁺ NK-92 cells with CD56 expression depicted along the y-axis and CD107a along the x-axis. Percentages of CD107a⁺ cells and CD107a mean fluorescence intensities (MFI) are noted. **(B)** Percentage decreased degranulation was calculated by the formula: $100\% \times ((\text{CD107a}^+ \% \times \text{MFI from Rab27A WT-transduced NK-92 cells}) - (\text{CD107a}^+ \% \times \text{MFI from Rab27A p.A87P-transduced NK-92 cells})) / (\text{CD107a}^+ \% \times \text{MFI from Rab27A WT-transduced NK-92 cells})$. The bar graph shows the means \pm SEM from three independent experiments. **(C)** NK-92 cells transduced with lentiviruses expressing Rab27A WT (*top panel*) or Rab27A p.A87P (*bottom panel*) were incubated with CFSE-labeled K562 target cells. Confocal microscopy portrays granzyme B (present only in NK-92 cells) as pink to orange in color, F-actin as blue, and both NK-92 and K562 cells as green. The arrow in the *top panel* denotes NK-92 cell granzyme B polarization to the immunologic synapse formed with the K562 target cell, whereas the arrow in the *lower panel* points to an NK-92 cell bound to a K562 cell but lacking granzyme B polarization to the immunologic synapse. Scale bar, 20 μm .

(Fig. 7). As this was a single snapshot in time, granzyme B polarization to the immunologic synapse with K562 target cells was further explored by a time course analysis.

Rab27A-expressing lentivirus-transduced NK-92 cells were incubated 2:1 with K562 target cells for variable time periods, spun down to slides, and fixed as in Fig. 6. Nuclei from both cell types were identified by DAPI (blue) staining, and granzyme B, present only in the NK-92 cells, was detected with fluorochrome (green)-tagged anti-granzyme B mAb (Fig. 8A). Two hundred cells per condition/per time point were counted (assessor blinded to time point and condition), and percentages of polarized cells (see *Materials and Methods*) were calculated for several experiments and graphed over a time course (Fig. 8B). Cells overexpressing Rab27A WT polarized granzyme B at a higher rate during the first hour compared with empty vector control-transduced NK-92 cells. In contrast, NK-92 cells transduced with a lentivirus expressing Rab27A p.A87P displayed delayed kinetics of polarization, not reaching control values for 2–4 h. To our knowledge, this is the first such demonstration of a heterozygous HLH gene mutation significantly delaying cytolytic vesicle polarization to the immunologic synapse. Thus, the patients' mutant Rab27A protein acted in a partial dominant-negative fashion to delay granzyme B delivery to the immunologic synapse, leading to decreased NK cell lytic function. It is likely that this delay in cytotoxic granule polarization results in decreased target cell lysis, prolonged engagement between the lytic and target cells, and increased proinflammatory cross-talk between the lymphocyte (CD8 T cell or NK cell) and the APC *in vivo* (25). Supportive of this, evaluation of intracellular cytokine levels revealed statistically significant increased IFN- γ expression in the mutant Rab27A p.A87P-transduced versus WT Rab27A-transduced NK-92 cells incubated with K562 target cells for 4–8 h (Fig. 9).

Rab27A p.A87P inhibits cytolytic function of unmanipulated patient-derived NK cells

To explore the effect of the Rab27A p.A87P mutation on the sHLH patients' own naturally occurring NK cells during a state of health, PBMCs were isolated from the Italian patient's peripheral blood,

along with blood from his father (Rab27A p.A87P heterozygote), mother (Rab27A WT), sister (Rab27A WT), and three unrelated healthy adult controls. PBMCs were incubated with K562 target cells, and NK cells (CD56⁺, CD3⁻) were analyzed for degranulation (CD107a expression) at varying E:T ratios. With increasing stimulus from K562 target cells (decreasing E:T ratios), there was a trend for increased degranulation of NK cells (Fig. 10A). Notably, the percentage of NK cells from both the Italian patient and his father (both heterozygous for Rab27A p.A87P) capable of degranulation was significantly decreased compared with NK cells from the patient's mother and sister (both WT Rab27A). Thus, NK cell function was decreased in unmanipulated heterozygous Rab27A p.A87P NK cells from peripheral blood, even during a state of good health.

Similarly, heterozygous Rab27A p.A87P NK cells from both the Italian sHLH patient and his father demonstrated significantly reduced NK cell lytic activity versus K562 target cells in comparison with NK cells from healthy adult controls (Fig. 10B). NK cell lytic activity was ~50% reduced for Rab27A p.A87P-expressing NK cells at all E:T ratios studied. Again, the sHLH patient's NK cells were analyzed at time of good health (two separate time points averaged), demonstrating decreased NK cell lytic activity at baseline. In general, there was no substantial difference in intracellular perforin levels in NK cells from the patient and his father in comparison with a healthy control and the patient's mother and sister (Supplemental Fig. 3). However, addition of IL-6 notably lowered perforin levels in those with and without the Rab27A p.A87P mutation, consistent with decreased cytolytic activity of the NK-92 cells incubated with IL-6 (Fig. 2C), as well as a recent publication (31). Thus, it is likely that the Rab27A p.A87P contributes to decreased NK cell function and subsequent sHLH clinical expression. However, the mutation alone is not sufficient to cause sHLH, as the patient's father expresses the same mutation, resulting in decreased NK cell function but no clinically overt sHLH, which may require an inflammatory milieu. Similarly, the Italian Rab27A p.A87P sHLH patient is not chronically ill with sHLH despite baseline decreased NK cell function.

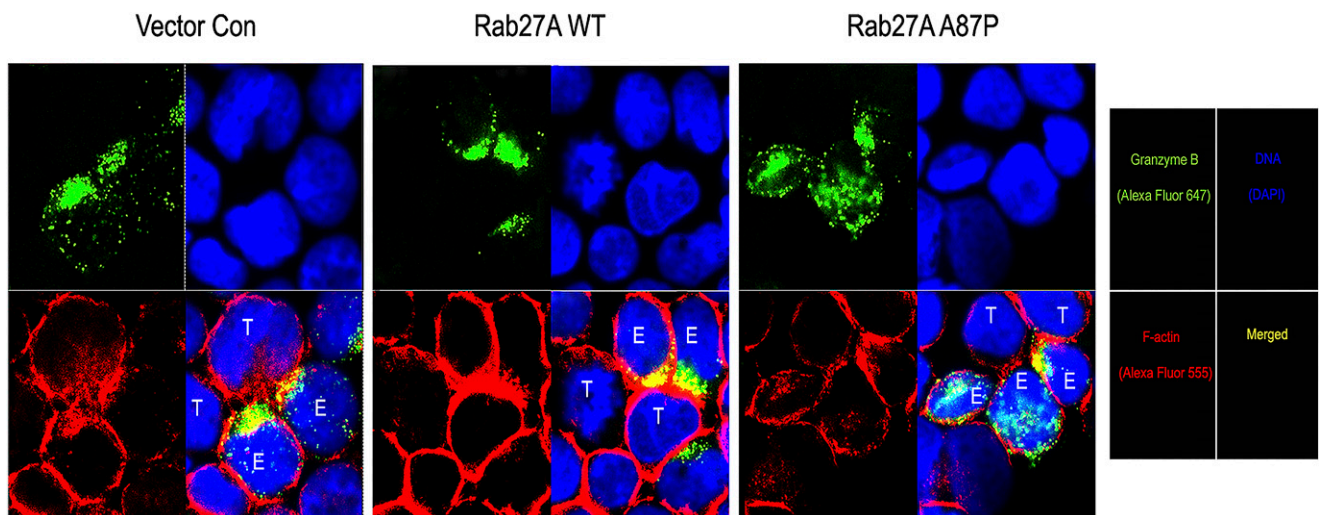


FIGURE 7. Polarization of granzyme B occurs at the plasma membrane of the immunologic synapse between NK-92 effector (E) cells and K562 target (T) cells but is decreased in those expressing mutant Rab27A p.A87P. NK-92 effector (E) cells transduced with lentiviruses expressing empty vector control (*left*), Rab27A WT (*middle*), or mutant Rab27A p.A87P (*right*) were mixed with K562 target (T) cells and assayed for granzyme B polarization to the plasma membrane at the immunological synapse by confocal microscopy (original magnification $\times 630$). Granzyme B is noted in green (*top left panels*), DNA (DAPI nuclear stain) in blue (*upper right panels*), and F-actin cytoskeleton (defining cell membranes) in red (*lower left panels*). Merged images of granzyme B, DNA, and F-actin are presented in the *bottom right panels* with yellow representing granzyme B and F-actin overlap, and light blue depicting granzyme B not polarized to the cell membrane immunological synapse.

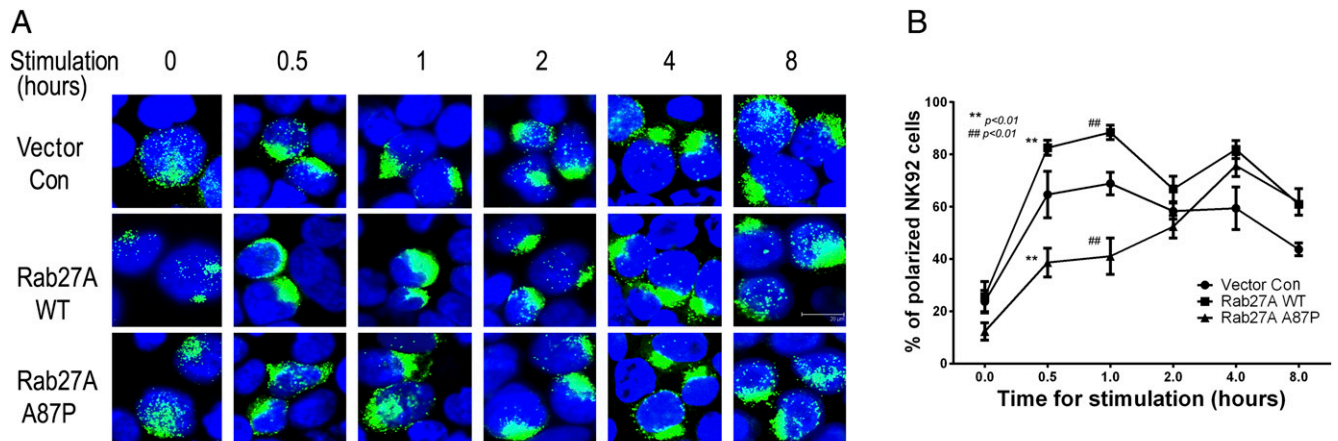


FIGURE 8. Rab27A p.A87P mutation delays granzyme B polarization to the immunologic synapse. **(A)** Vector control (*top row*), Rab27A WT (*middle*), and Rab27A p.A87P mutant (*bottom*)–transduced NK-92 cells were stimulated with K562 cells for the indicated time periods prior to intracellular analysis of granzyme B polarization as assessed by confocal microscopy. One representative experiment is shown, where green represents granzyme B staining and blue denotes cell nuclei (DAPI stain). Scale bar, 20 μ m. **(B)** Three independent experiments are summarized and plotted as percentages (*y*-axis) of granzyme B–polarized NK-92 cells (means \pm SEM) versus time (*x*-axis) for vector control (●), Rab27A WT (■), and Rab27A p.A87P (▲) expressing lentivirus-transduced cells. Statistically significant differences ($p < 0.0001$) in the means of granzyme B–polarized cells between the Rab27A WT– and Rab27A A87–expressing NK-92 cells is noted by two-way ANOVA analysis for the 0.5 and 1.0 h time points.

Discussion

fHLH and sHLH or MAS likely represent the same disorder along a spectrum of hyperinflammation and genetics (17, 40). Historically, those patients presenting early in life with homozygous and compound heterozygous mutations of HLH-causing genes have been classified as having fHLH, even when the inflammatory cascade initiation was secondary to a known infectious cause. Those lacking family history or known genetic mutations were previously classified as having acquired, reactive, or sHLH (41). However, recent reports have detailed many later onset sHLH and MAS patients found to have heterozygous mutations of the same fHLH-causing genes (17–20, 22–24, 42–44), although without any

supporting functional or mechanistic analyses of the effects of these heterozygous mutants, except for a few studies (17, 24, 42).

Mutations in HLH genes among sHLH and MAS patients are not likely coincidental, in part based on their relatively high frequency among these cohorts compared with the background population (17, 23, 45), but also because of their ability to act in a hypomorphic or partially dominant-negative fashion on NK cell cytolytic capacity (Fig. 2A, 2B) (17). Moreover, decreased lytic activity in the presence of IL-6 (Fig. 2C) may synergize with heterozygous partial dominant-negative, or hypomorphic, fHLH gene mutations to lead to clinical sHLH. Consistent with these findings, excess IL-6 (in vivo and in vitro) has been observed to

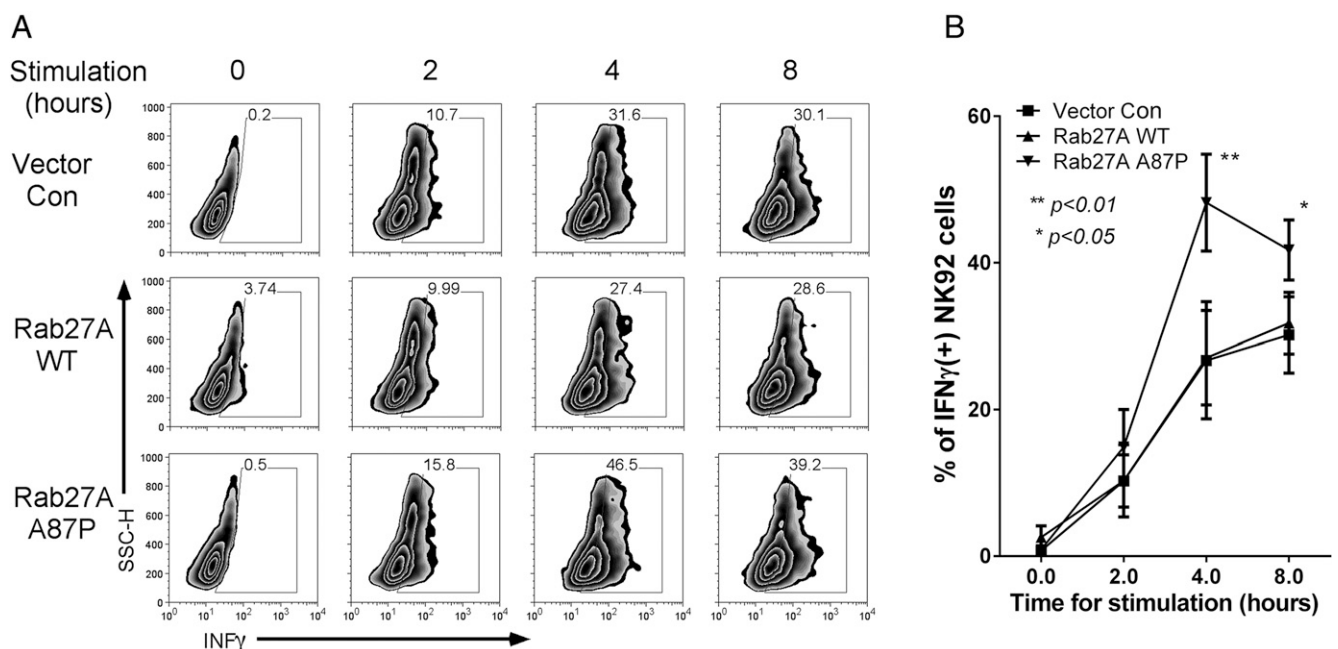


FIGURE 9. Increased IFN- γ expression by mutant Rab27A p.A87P, compared with WT Rab27A, expressing NK-92 cells following incubation of K562 target cells. **(A)** Empty vector (Con), mutant Rab27A p.A87P, or WT Rab27A lentivirus–transduced NK-92 cells were incubated with K562 cells for 4 h, and intracellular IFN- γ levels of GFP⁺ NK-92 cells are plotted (*x*-axis) versus side scatter (*y*-axis) for one representative experiment. **(B)** Average IFN- γ levels (means \pm SEM) are plotted for three similar experiments.

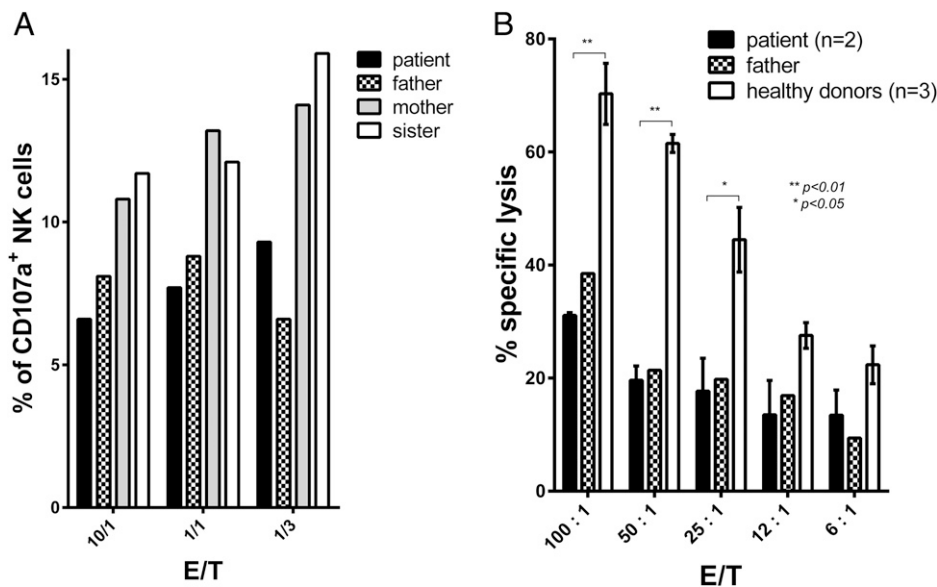


FIGURE 10. Heterozygous Rab27A p.A87P patient NK cells have decreased degranulation and cytotoxicity. **(A)** PBMCs were obtained from the heterozygous Rab27A p.A87P sHLH Italian patient (black bar), his Rab27 p.A87P heterozygous father (checkered bar), his Rab27A WT mother (gray bar), and his Rab27A WT sister (white bar). PBMCs were mixed with K562 cells at various E:T ratios as in *Materials and Methods*. Percentages of NK cells undergoing degranulation (CD107⁺, CD56⁺, CD3⁻) were determined by FCM. **(B)** PBMCs were obtained from the heterozygous Rab27A p.A87P sHLH Italian patient (at two time points during a 24-mo period of disease inactivity; black bar), his Rab27A p.A87P heterozygous father (single time point; checkered bar), and from three normal healthy unrelated control individuals (white bar). Cell lysis of NK-sensitive K562 cells was analyzed at various E:T ratios as detailed in *Materials and Methods*. Error bars represent means \pm SEM for the patient (two time points) and the average of the three controls.

decrease NK cell activity with decreased granzyme B and perforin expression in murine and human NK cells (31). This may be particularly relevant to MAS in the setting of systemic juvenile idiopathic arthritis where IL-6 is often elevated, and heterozygous fHLH gene mutations are frequently present in those with MAS (15). Nevertheless, one cannot formally rule out the possibility of not identifying other contributory genes leading to decreased NK cell function, or not identifying causative mutations or deletions in non-coding portions of HLH genes among sHLH and MAS patients (46). However, the fact that isolated overexpression of the Rab27A p.A87P mutation in an NK-92 cell possessing the Rab27A WT gene is able to delay granzyme B polarization to the immunologic synapse (Fig. 8) and decrease NK cell lytic function (Fig. 2) argues that these genes may directly contribute to HLH pathophysiology as single copy mutations. Analogous decreased NK cell function has recently been reported for overexpression of a novel Munc18-2 mutation associated with a fatal case of sHLH in a teenager (17). Thus, single copy mutations in fHLH genes (identified in sHLH patients) introduced into NK cells can act in a partially dominant-negative fashion to disrupt NK cell function and likely directly contribute to sHLH or MAS pathology under certain inflammatory states (e.g., particular viral infections, lymphoma, autoimmune or autoinflammatory disease flares) (47).

In the present study, we explore the mechanism for the heterozygous Rab27A p.A87P mutation contributing to sHLH in two unrelated individuals. The decreased lytic activity of NK cells expressing Rab27A p.A87P likely results from the mutation disrupting interaction with its binding partner, Munc13-4 (Figs. 4, 5, Supplemental Fig. 2). The Rab27A p.A87P mutation resides along the highly conserved Rab protein switch 2 region, critical for interaction with Munc13-4 and its homologs in other tissues (Fig. 4). The decreased interaction of Rab27A p.A87P with WT Munc13-4 (Fig. 5, Supplemental Fig. 2) likely occurs via a partial dominant-negative effect leading to inhibition of cytolytic granule exocytosis, because the Rab27A p.A87P mutant probably effectively competes with WT Rab27A for other binding partners in the

exocytosis pathway. Similarly, a Rab27A p.G78L mutation, which also resides along the switch 2 region, was shown to inhibit lymphocyte cytotoxic granule exocytosis via a dominant-negative effect (48). The decreased interaction of Rab27 p.A87P with Munc13-4 results in a delay of NK cell cytolytic granule polarization to the immunologic synapse (Fig. 8). The delay in polarization occurs as early as 30 min after interaction with the K562 target cells (Fig. 7B) but without disrupting the interaction of the NK cells with the target cells (Fig. 3), including several hours after incubation (Supplemental Fig. 4).

Recently, it has been shown that NK cells or cytotoxic CD8 T cells homozygous deficient in either granzyme B or perforin delay separation from their target cells with an \sim 5-fold longer interaction at the immunologic synapse (25). Interestingly, the absence of cell lysis prevents the disengagement of the cells, as this occurs via a caspase-dependent mechanism from the dying target cell (25). This prolonged interaction of the lytic cell and the target cell results in hypersecretion of proinflammatory cytokines (IL-6, TNF, IFN- γ) and thus provides a link between failed perforin-mediated cytolytic activity and the cytokine storm responsible for clinical HLH (25). Therefore, it is reasonable to conclude that a mutation (Rab27A p.A87P) that delays cytolytic granule polarization to the plasma membrane of the immunologic synapse (Figs. 7, 8) and decreases target cell death (Figs. 2, 10) likely leads to prolonged interaction of cytolytic lymphocytes with APCs, resulting in a proinflammatory cytokine storm (Fig. 9) responsible for clinical manifestations of sHLH.

The distinction between sHLH/MAS and fHLH currently determines treatment decisions. Patients diagnosed with fHLH have typically been treated with cytotoxic agents, namely etoposide, and hematopoietic stem cell transplant (5), with a 5-y survival for both fHLH and sHLH/MAS patients of only 55%. In contrast, some patients with MAS and its variants have been treated by targeting the hyperinflammatory state acutely with high dose CS, CsA, and IL-1 blockade (Fig. 1) (14), including effective IL-1 blockade in sepsis patients with features of MAS (49). This treatment

approach has yet to be evaluated in a large prospective MAS cohort, but uncontrolled studies report that short-term survival is >85%; long-term survival data are not yet currently available (14, 17). The patients reported in this study have been clinically stable for 3 and 5 y, respectively, after their initial MAS presentations and have received minimal to no immunosuppression for the last 3 y. Nonetheless, the place of hematopoietic stem cell transplantation in this group of patients with heterozygous mutations in HLH-associated genes remains unclear. These patients are theoretically at risk for developing recurrent MAS under certain hyperinflammatory states (e.g., certain viral infections). However, a relatively rapid and apparently sustained response to a limited course of immunosuppression without the use of cytotoxic agents suggests that transplantation may be unnecessary in many sHLH and MAS patients, even in the face of heterozygosity of known disease-causing mutations. Further follow-up of patients with sHLH and MAS who respond to immunosuppressive therapy alone is needed to determine the rate of recurrence of sHLH and MAS and the subsequent response to therapy.

In conclusion, we identified a heterozygous *RAB27A* known Griscelli 2 missense mutation (*c.259G→C*) in two previously healthy unrelated teenagers who each presented with sHLH. Overexpression of this single copy HLH gene mutation in a human NK cell line resulted in decreased degranulation, diminished interaction with its Munc13-4 binding partner, delayed polarization of granzyme B to the immunologic synapse, increased IFN- γ expression, and reduced cytolytic function. Decreased NK cell lytic activity was noted in naturally occurring (patient derived) heterozygous Rab27A p.A87P NK cells at baseline, arguing for the requirement of an additional trigger to result in clinically evident sHLH. When sHLH was clinically severe, both Rab27A p.A87P heterozygous patients responded to immunosuppression and have not required traditional etoposide-based treatment or bone marrow transplantation up to 5 y after initial presentation. Thus, the identification of partially dominant-negative single copy gene mutations in late-onset sHLH blurs the genetic distinction between fHLH and sHLH, underscores the increased prevalence of sHLH and MAS compared with fHLH, and poses an additional consideration in choosing the safest effective therapy for sHLH and MAS patients with or without heterozygous HLH gene mutations.

Acknowledgments

We thank the patients and their parents and sibling for participation in this research.

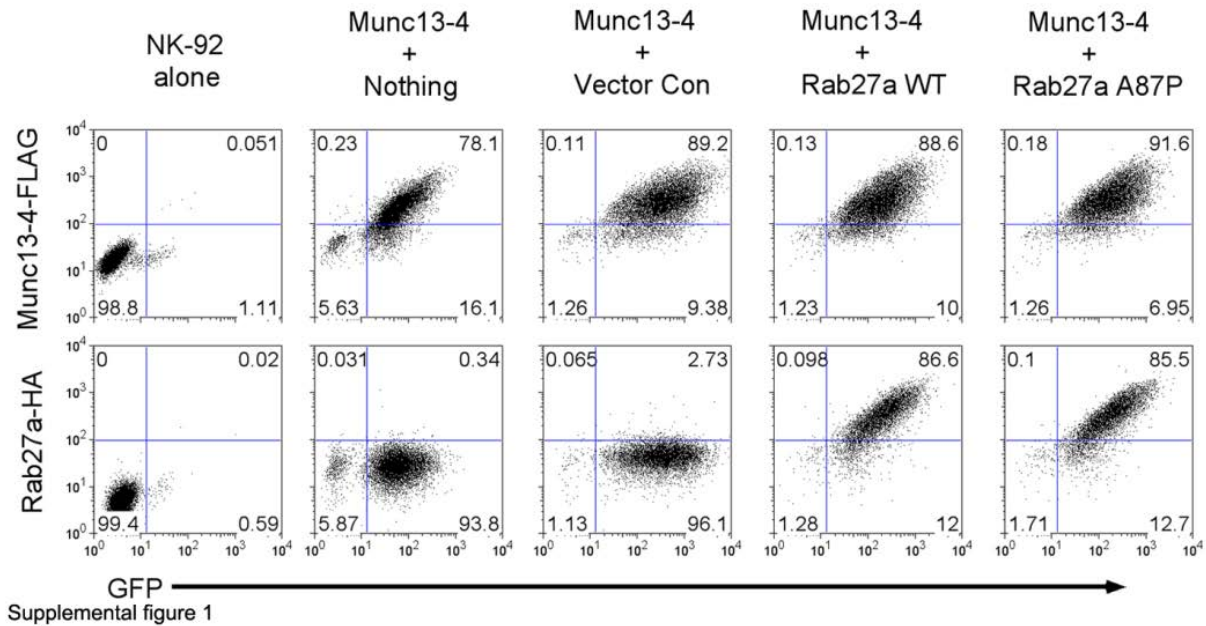
Disclosures

The authors have no financial conflicts of interest.

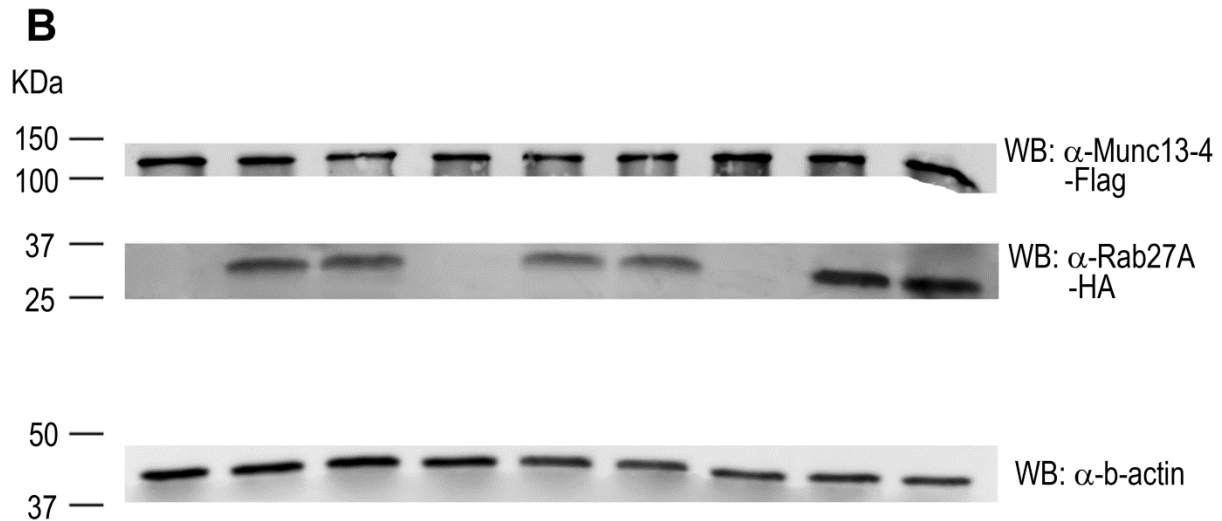
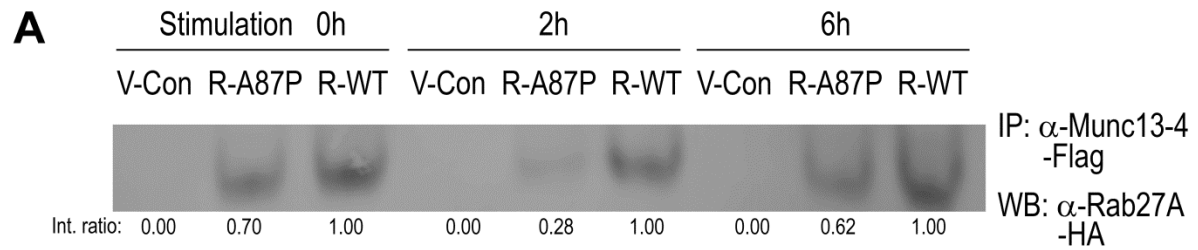
References

- Janka, G. E. 2012. Familial and acquired hemophagocytic lymphohistiocytosis. *Annu. Rev. Med.* 63: 233–246.
- Freeman, H. R., and A. V. Ramanan. 2011. Review of haemophagocytic lymphohistiocytosis. *Arch. Dis. Child.* 96: 688–693.
- Behrens, E. M. 2008. Macrophage activation syndrome in rheumatic disease: what is the role of the antigen presenting cell? *Autoimmun. Rev.* 7: 305–308.
- Fisman, D. N. 2000. Hemophagocytic syndromes and infection. *Emerg. Infect. Dis.* 6: 601–608.
- Henter, J. I., A. Horne, M. Aricó, R. M. Egeler, A. H. Filipovich, S. Imashuku, S. Ladisch, K. McClain, D. Webb, J. Winiarski, and G. Janka. 2007. HLH-2004: diagnostic and therapeutic guidelines for hemophagocytic lymphohistiocytosis. *Pediatr. Blood Cancer* 48: 124–131.
- Henter, J. I., A. Samuelsson-Horne, M. Aricó, R. M. Egeler, G. Elinder, A. H. Filipovich, H. Gadner, S. Imashuku, D. Komp, S. Ladisch, et al; Histiocyte Society. 2002. Treatment of hemophagocytic lymphohistiocytosis with HLH-94 immunochemotherapy and bone marrow transplantation. *Blood* 100: 2367–2373.
- Deane, S., C. Selmi, S. S. Teuber, and M. E. Gershwin. 2010. Macrophage activation syndrome in autoimmune disease. *Int. Arch. Allergy Immunol.* 153: 109–120.
- Cron, R. Q., S. Davi, F. Minoia, and A. Ravelli. 2015. Clinical features and correct diagnosis of macrophage activation syndrome. *Expert Rev. Clin. Immunol.* 11: 1043–1053.
- Fardet, L., L. Galicier, O. Lambotte, C. Marzac, C. Aumont, D. Chahwan, P. Coppo, and G. Hejblum. 2014. Development and validation of the HScore, a score for the diagnosis of reactive hemophagocytic syndrome. *Arthritis Rheumatol.* 66: 2613–2620.
- Ringold, S., P. F. Weiss, T. Beukelman, E. M. DeWitt, N. T. Ilowite, Y. Kimura, R. M. Laxer, D. J. Lovell, P. A. Nigrovic, A. B. Robinson, and R. K. Vehe. American College of Rheumatology. 2013. 2013 update of the 2011 American College of Rheumatology recommendations for the treatment of juvenile idiopathic arthritis: recommendations for the medical therapy of children with systemic juvenile idiopathic arthritis and tuberculosis screening among children receiving biologic medications. *Arthritis Rheum.* 65: 2499–2512.
- Bruck, N., M. Suttrop, M. Kabus, G. Heubner, M. Gahr, and F. Pessler. 2011. Rapid and sustained remission of systemic juvenile idiopathic arthritis-associated macrophage activation syndrome through treatment with anakinra and corticosteroids. *J. Clin. Rheumatol.* 17: 23–27.
- Kahn, P. J., and R. Q. Cron. 2013. Higher-dose anakinra is effective in a case of medically refractory macrophage activation syndrome. *J. Rheumatol.* 40: 743–744.
- Kelly, A., and A. V. Ramanan. 2008. A case of macrophage activation syndrome successfully treated with anakinra. *Nat. Clin. Pract. Rheumatol.* 4: 615–620.
- Miettinen, P. M., A. Narendran, A. Jayanthan, E. M. Behrens, and R. Q. Cron. 2011. Successful treatment of severe paediatric rheumatic disease-associated macrophage activation syndrome with interleukin-1 inhibition following conventional immunosuppressive therapy: case series with 12 patients. *Rheumatology (Oxford)* 50: 417–419.
- Ravelli, A., A. A. Grom, E. M. Behrens, and R. Q. Cron. 2012. Macrophage activation syndrome as part of systemic juvenile idiopathic arthritis: diagnosis, genetics, pathophysiology and treatment. *Genes Immun.* 13: 289–298.
- Record, J. L., T. Beukelman, and R. Q. Cron. 2011. Combination therapy of abatacept and anakinra in children with refractory systemic juvenile idiopathic arthritis: a retrospective case series. *J. Rheumatol.* 38: 180–181.
- Zhang, M., E. M. Behrens, T. P. Atkinson, B. Shakoory, A. A. Grom, and R. Q. Cron. 2014. Genetic defects in cytotoxicity in macrophage activation syndrome. *Curr. Rheumatol. Rep.* 16: 439–446.
- Zhang, K., J. Biroschak, D. N. Glass, S. D. Thompson, T. Finkel, M. H. Passo, B. A. Binstadt, A. Filipovich, and A. A. Grom. 2008. Macrophage activation syndrome in patients with systemic juvenile idiopathic arthritis is associated with MUNC13-4 polymorphisms. *Arthritis Rheum.* 58: 2892–2896.
- Hazen, M. M., A. L. Woodward, I. Hofmann, B. A. Degar, A. Grom, A. H. Filipovich, and B. A. Binstadt. 2008. Mutations of the hemophagocytic lymphohistiocytosis-associated gene UNC13D in a patient with systemic juvenile idiopathic arthritis. *Arthritis Rheum.* 58: 567–570.
- Vastert, S. J., R. van Wijk, L. E. D'Urbano, K. M. de Vooght, W. de Jager, A. Ravelli, S. Magni-Manzoni, A. Insalaco, E. Cortis, W. W. van Solinge, et al. 2010. Mutations in the perforin gene can be linked to macrophage activation syndrome in patients with systemic onset juvenile idiopathic arthritis. *Rheumatology (Oxford)* 49: 441–449.
- Zhizhuo, H., X. Junmei, S. Yuelin, Q. Qiang, L. Chunyan, X. Zhengde, and S. Kunling. 2012. Screening the PRF1, UNC13D, STX11, SH2D1A, XIAP, and ITK gene mutations in Chinese children with Epstein-Barr virus-associated hemophagocytic lymphohistiocytosis. *Pediatr. Blood Cancer* 58: 410–414.
- Sieni, E., V. Cetica, A. Piccin, F. Gherlinzoni, F. C. Sasso, M. Rabusin, L. Attard, A. Bosi, D. Pende, L. Moretta, and M. Aricó. 2012. Familial hemophagocytic lymphohistiocytosis may present during adulthood: clinical and genetic features of a small series. *PLoS One* 7: e44649.
- Zhang, K., M. B. Jordan, R. A. Marsh, J. A. Johnson, D. Kissell, J. Meller, J. Villanueva, K. A. Risma, Q. Wei, P. S. Klein, and A. H. Filipovich. 2011. Hypomorphic mutations in PRF1, MUNC13-4, and STXBP2 are associated with adult-onset familial HLH. *Blood* 118: 5794–5798.
- Spessott, W. A., M. L. Sanmillan, M. E. McCormick, N. Patel, J. Villanueva, K. Zhang, K. E. Nichols, and C. G. Giraudo. 2015. Hemophagocytic lymphohistiocytosis caused by dominant-negative mutations in STXBP2 that inhibit SNARE-mediated membrane fusion. *Blood* 125: 1566–1577.
- Jenkins, M. R., J. A. Rudd-Schmidt, J. A. Lopez, K. M. Ramsbottom, S. I. Mannerling, D. M. Andrews, I. Voskoboinik, and J. A. Trapani. 2015. Failed CTL/NK cell killing and cytokine hypersecretion are directly linked through prolonged synapse time. *J. Exp. Med.* 212: 307–317.
- Gong, J. H., G. Maki, and H. G. Klingemann. 1994. Characterization of a human cell line (NK-92) with phenotypic and functional characteristics of activated natural killer cells. *Leukemia* 8: 652–658.
- Selliah, N., M. Zhang, S. White, P. Zoltick, B. E. Sawaya, T. H. Finkel, and R. Q. Cron. 2008. FOXP3 inhibits HIV-1 infection of CD4 T-cells via inhibition of LTR transcriptional activity. *Virology* 381: 161–167.
- Endo, M., P. W. Zoltick, W. H. Peranteau, A. Radu, N. Muvarak, M. Ito, Z. Yang, G. Cotsarelis, and A. W. Flake. 2008. Efficient in vivo targeting of epidermal stem cells by early gestational intraamniotic injection of lentiviral vector driven by the keratin 5 promoter. *Mol. Ther.* 16: 131–137.
- Klein, E., H. Ben-Bassat, H. Neumann, P. Ralph, J. Zeuthen, A. Polliack, and F. Vánky. 1976. Properties of the K562 cell line, derived from a patient with chronic myeloid leukemia. *Int. J. Cancer* 18: 421–431.
- Bryceson, Y. T., D. Pende, A. Maul-Pavicic, K. C. Gilmour, H. Ufheil, T. Vraetz, S. C. Chiang, S. Marcenaro, R. Meazza, I. Bondzio, et al. 2012. A prospective evaluation of degranulation assays in the rapid diagnosis of familial hemophagocytic syndromes. *Blood* 119: 2754–2763.

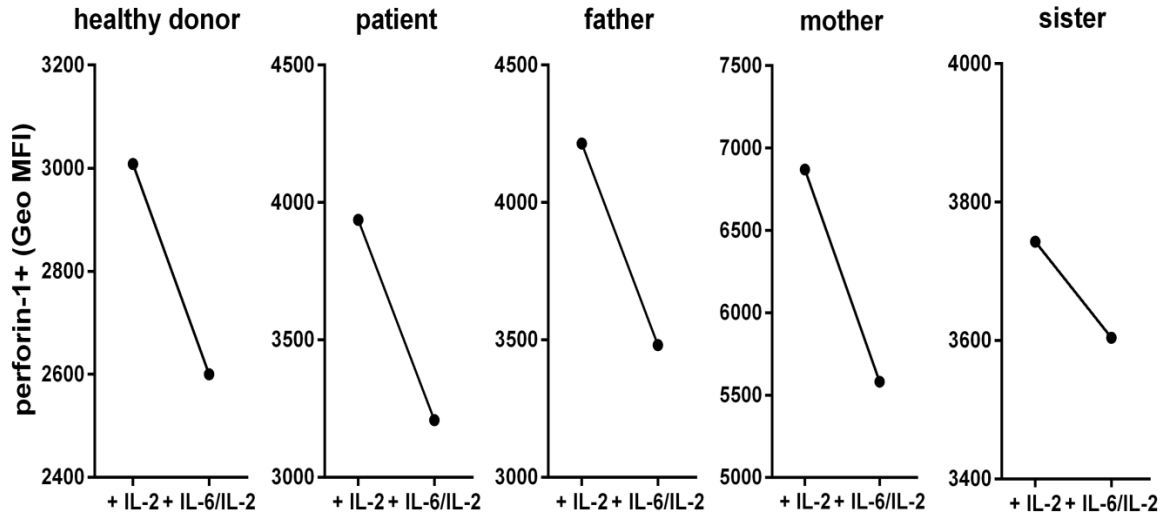
31. Cifaldi, L., G. Prencipe, I. Caiello, C. Bracaglia, F. Locatelli, F. De Benedetti, and R. Strippoli. 2015. Inhibition of natural killer cell cytotoxicity by interleukin-6: implications for the pathogenesis of macrophage activation syndrome. *Arthritis Rheumatol.* 67: 3037–3046.
32. Chavas, L. M., K. Ihara, M. Kawasaki, S. Torii, T. Uejima, R. Kato, T. Izumi, and S. Wakatsuki. 2008. Elucidation of Rab27 recruitment by its effectors: structure of Rab27a bound to Exophilin4/Slp2-a. *Structure* 16: 1468–1477.
33. Kukimoto-Niino, M., A. Sakamoto, E. Kanno, K. Hanawa-Suetsugu, T. Terada, M. Shirouzu, M. Fukuda, and S. Yokoyama. 2008. Structural basis for the exclusive specificity of Slac2-a/melanophilin for the Rab27 GTPases. *Structure* 16: 1478–1490.
34. Wulf, E., A. Deboen, F. A. Bautz, H. Faulstich, and T. Wieland. 1979. Fluorescent phalloxin, a tool for the visualization of cellular actin. *Proc. Natl. Acad. Sci. USA* 76: 4498–4502.
35. Gorelik, M., K. S. Torok, D. A. Kietz, and R. Hirsch. 2011. Hypocomplementemia associated with macrophage activation syndrome in systemic juvenile idiopathic arthritis and adult onset still's disease: 3 cases. *J. Rheumatol.* 38: 396–397.
36. Zur Stadt, U., K. Beutel, S. Kolberg, R. Schneppenheim, H. Kabisch, G. Janka, and H. C. Hennies. 2006. Mutation spectrum in children with primary hemophagocytic lymphohistiocytosis: molecular and functional analyses of PRF1, UNC13D, STX11, and RAB27A. *Hum. Mutat.* 27: 62–68.
37. Caiello, I., G. Minnone, D. Holzinger, T. Vogl, G. Prencipe, A. Manzo, F. De Benedetti, and R. Strippoli. 2014. IL-6 amplifies TLR mediated cytokine and chemokine production: implications for the pathogenesis of rheumatic inflammatory diseases. *PLoS One* 9: e107886.
38. Ohbayashi, N., S. Mamishi, K. Ishibashi, Y. Maruta, B. Pourakbari, B. Tamizifar, M. Mohammadpour, M. Fukuda, and N. Parvaneh. 2010. Functional characterization of two RAB27A missense mutations found in Griscelli syndrome type 2. *Pigment Cell Melanoma Res.* 23: 365–374.
39. Orange, J. S. 2008. Formation and function of the lytic NK-cell immunological synapse. *Nat. Rev. Immunol.* 8: 713–725.
40. Ramanan, A. V., and R. Schneider. 2003. Macrophage activation syndrome—what's in a name! *J. Rheumatol.* 30: 2513–2516.
41. Athreya, B. H. 2002. Is macrophage activation syndrome a new entity? *Clin. Exp. Rheumatol.* 20: 121–123.
42. Risma, K. A., R. W. Frayer, A. H. Filipovich, and J. Sumegi. 2006. Aberrant maturation of mutant perforin underlies the clinical diversity of hemophagocytic lymphohistiocytosis. *J. Clin. Invest.* 116: 182–192.
43. Unal, S., G. Balta, H. Okur, S. Aytac, M. Cetin, F. Gumruk, S. Ozen, and A. Gurgey. 2013. Recurrent macrophage activation syndrome associated with heterozygous perforin W374X gene mutation in a child with systemic juvenile idiopathic arthritis. *J. Pediatr. Hematol. Oncol.* 35: e205–e208.
44. Wang, Y., Z. Wang, J. Zhang, Q. Wei, R. Tang, J. Qi, L. Li, L. Ye, J. Wang, and L. Ye. 2014. Genetic features of late onset primary hemophagocytic lymphohistiocytosis in adolescence or adulthood. *PLoS One* 9: e107386.
45. Molleran Lee, S., J. Villanueva, J. Sumegi, K. Zhang, K. Kogawa, J. Davis, and A. H. Filipovich. 2004. Characterisation of diverse PRF1 mutations leading to decreased natural killer cell activity in North American families with hemophagocytic lymphohistiocytosis. *J. Med. Genet.* 41: 137–144.
46. Cichocki, F., H. Schlums, H. Li, V. Stache, T. Holmes, T. R. Lenvik, S. C. Chiang, J. S. Miller, M. Meeths, S. K. Anderson, and Y. T. Bryceson. 2014. Transcriptional regulation of Munc13-4 expression in cytotoxic lymphocytes is disrupted by an intronic mutation associated with a primary immunodeficiency. *J. Exp. Med.* 211: 1079–1091.
47. Schulert, G. S., M. Zhang, N. Fall, A. Husami, D. Kissell, A. Hanosh, K. Zhang, K. Davis, J. M. Jentzen, L. Napolitano, et al. 2015. Whole-exome sequencing reveals mutations in genes linked to hemophagocytic lymphohistiocytosis and macrophage activation syndrome in fatal cases of H1N1 influenza. *J. Infect. Dis.* jiv550.
48. Menasche, G., J. Feldmann, A. Houdusse, C. Desaymard, A. Fischer, B. Goud, and G. de Saint Basile. 2003. Biochemical and functional characterization of Rab27a mutations occurring in Griscelli syndrome patients. *Blood* 101: 2736–2742.
49. Shakoory, B., J. A. Carcillo, W. W. Chatham, R. L. Amdur, H. Zhao, C. A. Dinarello, R. Q. Cron, and S. M. Opal. 2016. Interleukin-1 receptor blockade is associated with reduced mortality in sepsis patients with features of macrophage activation syndrome: reanalysis of a prior phase III trial. *Crit. Care Med.* 44: 275–281.



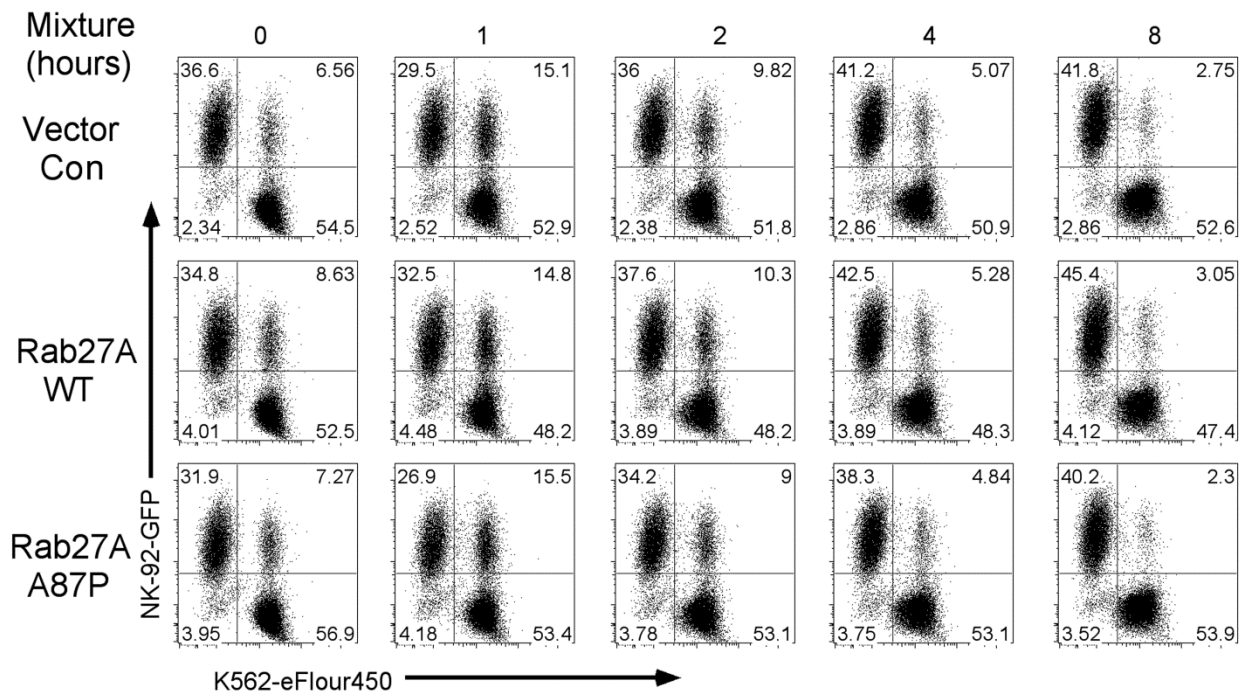
Supplemental Figure 1. Equivalent expression of WT and mutant Rab27A along with WT Munc13-4 by dual lentiviral transduction. Corresponding to the data presented in Figure 5, NK-92 cells (far left) were transduced with a GFP-expressing (X-axis) lentivirus co-expressing FLAG-tagged Munc13-4 WT alone (middle left) or, after sorting for GFP⁺ cells, followed by superinfection with GFP-expressing lentiviruses (X-axis) co-expressing nothing (middle), or HA-tagged Rab27A WT (middle right) or Rab27A p.A87P mutant (far right). Munc13-4 expression (top row) was detected by FCM with anti-FLAG antibody (Y-axis), whereas Rab27A (WT or mutant) expression (bottom row) was detected with anti-HA antibody (Y-axis). One representative experiment of 3 is presented.



Supplemental Figure 2. Decreased co-immunoprecipitation of WT Munc13-4 with mutant Rab27A p.A87P. NK-92 cells were transduced with WT Munc13-4 plus GFP co-expressing empty vector control (V-Con), mutant Rab27A p.A87P (R-A87P), or WT Rab27A (R-WT) lentiviral vectors, and GFP⁺ cells were sorted by FCM as described in the Methods. The 3 groups of sorted GFP⁺ NK-92 cells were incubated with K562 target cells for 0, 2, and 6 hours, and protein lysates were extracted. Protein extracts were immunoprecipitated with anti-FLAG mAb (detects exogenous WT Munc13-4) and eluted precipitates were electrophoresed on agarose gels. (A) The gel blots were probed with anti-HA mAb (detects exogenous mutant and WT Rab27A) and bands were quantified by densitometry. The intensity ratios (Int. ratio) of the mutant Rab27A bands were calculated relative to the corresponding time point bands from WT Rab27A (designated 1.00) using ImageJ2 software, with the empty vector control serving as background (0.00). (B) Control Western blots for expression of transduced Munc13-4 and Rab27A, as well as endogenous β -actin, demonstrate equivalent levels of transduced lentiviral vectors (n=3).



Supplemental Figure 3. Perforin levels in Rab27A patient derived NK cells. PBMC were isolated from a healthy control, the Italian patient (Rab27A p.A87P), his father (Rab27A p.A87P), mother (Rab27A WT), and sister (Rab27A). PBMCs were cultured with or without hIL-6 and soluble hIL-6 receptor. After 24 hours of incubation at 37°C in the presence or in the absence of IL-6/sIL-6R, IL-2 was added to the medium, and cells were incubated for a further 24 hours. Intracellular perforin expression in the NK cell subset (CD56⁺CD3⁻) was evaluated by FCM (see Methods). The geometric mean fluorescence intensity (MFI) staining of perforin is plotted on the Y-axis for NK cells incubated in the presence of IL-2 with or without IL-6 for each of the 5 individuals examined.



Supplemental Figure 4. Rab27A p.A87P mutation does not alter NK cell conjugation formation with target cells at later time points post-incubation. As in Figure 3, NK-92 cells transduced with lentiviruses co-expressing GFP and empty vector control (top), Rab27A WT (middle), or Rab27A p.A87P (bottom) were mixed with eFluor450-labeled K562 cells and assayed for cell-to-cell conjugation as assessed by FCM. GFP expression (NK-92 cells) is shown along the Y-axis and eFluor450 fluorescence (K562 cells) along the X-axis. NK-92-K562 cell conjugates are noted in the upper right quadrants, and percentages of cells in each quadrant are noted. Cell conjugate formation was analysed at 0, 1, 2, 4, and 8 hours post-incubation of NK-92 and K562 cells. The results shown are representative of 3 similar experiments.